MDPI

Article

Robust Combined Adaptive Passivity-Based Control for Induction Motors

Juan Carlos Travieso-Torres [1,*], Abdiel Josadac Ricaldi-Morales [1] and Norelys Aguila-Camacho [2]

1   Industrial Technologies Department, University of Santiago of Chile, El Belloto 3735, Santiago 9170124, Chile; abdi.ricaldi@gmail.com
2   Department of Electricity, Universidad Tecnológica Metropolitana, José Pedro Alessandri 1242, Santiago 8330378, Chile; norelys.aguila@utem.cl
*   Correspondence: juancarlos.travieso@usach.cl; Tel.: +56-9-5629-2048

Abstract: The need for industrial and commercial machinery to maintain high torque while accurately following a variable angular speed is increasing. To meet this demand, induction motors (IMs) are commonly used with variable speed drives (VSDs) that employ a field-oriented control (FOC) scheme. Over the last thirty years, IMs have been replacing independent connection direct current motors due to their cost-effectiveness, reduced maintenance needs, and increased efficiency. However, IMs and VSDs exhibit nonlinear behavior, uncertainties, and disturbances. This paper proposes a robust combined adaptive passivity-based control (CAPBC) for this class of nonlinear systems that applies to angular rotor speed and stator current regulation inside an FOC scheme for IMs' VSDs. It uses general Lyapunov-based design energy functions and adaptive laws with σ-modification to assure robustness after combining control and monitoring variables. Lyapunov's second method and the Barbalat Lemma prove that the control and identification error tends to be zero over time. Moreover, comparative experimental results with a standard proportional–integral controller (PIC) and direct APBC show the proposed CAPBC's effectiveness and robustness under normal and changing conditions.

Keywords: robust adaptive systems; combined adaptive passivity-based control; field-oriented control; variable speed drives

1. Introduction

Since the late 1800s, machines used in industry and commerce have relied on direct current (DC) motors. Since the 20th century, DC variable speed drives (VSDs) have been used based on Thyristor rectifiers for high starting torque and variable speed accuracy. However, these DC motors tend to spark and are susceptible to threading, grooving, and flashover, as noted in [1]. As a result, induction motors (IMs), particularly the squirrel cage type, have gradually replaced them over the past three decades. IMs are more cost-effective and efficient and require less maintenance, as stated in [2]. Consequently, the sales of IMs have increased by 85%, accounting for 60% of the total electricity consumption in the industrial sector [2].

However, due to their nonlinear characteristics, alternating current (AC) VSDs are more complex than DC VSDs [2]. They require IGBT-based inverters to regulate the stator voltage and frequency. AC VSDs use three main control schemes: scalar control [3], direct torque control (DTC) [4,5], and field-oriented control (FOC) [6,7]. Nevertheless, the indirect FOC (IFOC) scheme [7] delivers higher output torque, higher stationary speed accuracy, and fast and nonoscillatory transient behavior. It performs more closely to DC's VSDs for the machinery under study in this manuscript.

The IFOC method simplifies the mathematical model of an IM by choosing a specific electrical angular slip. This simplification allows for the independent control of the electromagnetic torque and the rotor magnetic flux [8]. The basic IFOC relies on knowledge

of the rotor time constant (τ_r) and uses proportional–integral controllers (PICs). These PICs assume constant angular rotor speed operation and neglect disturbances such as load torque and the inverter model uncertainty to deal with simple linear dynamical systems (LDSs) [9]. Adjusting them also requires information on all the motor load parameters, which can be obtained from diverse methods [10], such as offline algorithms [11,12], offline tests [13,14], and self-commissioning tests [15,16].

Improving controller performance for FOC of IM has been a hot topic for the last decades and today [17–25]. The work in [20] proposes substituting the PICs with parallel PICs, improving robustness and performance indexes. However, [20] (Section 4) recognizes tuning difficulties with a doubled number of parameters, using genetic algorithms and particle swarm optimization (PSO) algorithms. The studies in [21,23] propose using a fractional-order PIC for the speed control outer loop, again with tuning issues for the fractional order value. The proposals in [24,25] design sliding mode controllers (SMCs), which are also nonadaptive depending on the parameter's knowledge. The review in [22] discusses this SMC issue and compares it with DMRAC, fuzzy, and artificial neural network (ANN) controllers. These last two need optimization techniques for minimal error, error adjustment, and membership function, with a more complex design and adjustment, as described in [22,26]. The proposed DAPBC [17] has a more straightforward design but still has tuning difficulties, depending on trial and error. The work in [27] enhances [17] by providing a specific formula depending on the operational range and not on the plant parameters for the DAPBC controller parameters tuning; however, it is not applied to FOC controllers.

It is clear that robust adaptive controllers ensure robustness under parameter variations without relying on their explicit knowledge [28–30]. There are three approaches to adaptive control—direct (D), indirect (I), and combined (C) [30]. The direct method is the most widely used. It has been applied to various applications such as self-piloted crafts [31–33], robotics [34–36], power systems [37,38], including induction motors [17,39,40]. However, the C method proposed in the work in [41] aims to improve the transient performance beyond the direct and indirect dynamic methods. Nevertheless, all these techniques have tuning issues. Therefore, this manuscript proposes a combined approach with a tuning method by expanding [27] with a tuning method.

In particular, the work in [41] introduced the C approach for the model reference adaptive control (MRAC) technique for scalar LDS. Later, ref. [42] applied CMRAC to pH control for a chemical reactor, outperforming a PID controller and DMRAC. The method was then extended to single-input and single-output (SISO) LDS by controlling longitudinal airplane movement [43]. These studies consider unknown plant parameters with the known sign of the input parameter b, referred to as the known control direction (KCD). The KCD assumes that the input parameter equals its unknown modulus multiplied by its known sign. This is valid for SISO plants and multiple-input multiple-output (MIMO) systems with a diagonal input matrix B, where $B = |B| sign(B)$, such as IMs.

On the other hand, refs. [44,45] propose a CMRAC for MIMO LDS. However, they assume a known input matrix B, substantially simplifying the adaptive control problem. Meanwhile, ref. [46] considered an adaptive control law with a known input matrix substituted by its estimate. Lastly, refs. [47,48] neglected the estimation error and considered an unknown input matrix to control uncrewed underwater and air vehicles, respectively. Hence, this manuscript uses the ideas originally proposed by CMRAC [41–43] to extend the D adaptive passivity-based control (APBC) technique [27], which ensures faster results than MRAC for the IFOC scheme.

As a contribution, this paper proposes a new control technique called CAPBC for a broader class of MIMO nonlinear linear dynamical systems (NLDSs). The proposed technique can handle systems with unmodeled dynamics and bounded external disturbance, including the case of IMs. The CAPBC considers the parameters closed-loop estimation error, first introduced by Duarte et al. [41]. To ensure robustness, the CAPBC incorporates a MIMO sigma-modification [28–30]. The proposed technique was applied to the outer and

inner controllers of an IFOC scheme for IMs and tested in a laboratory. The contributions of this proposal are detailed as follows:

1. **Proposing a novel CAPBC.** This paper proposes a novel CAPBC technique that extends the existing DAPBC scheme from [27]. Compared with previous works [41–43], the CAPBC can handle a wider range of MIMO NLDS with bounded external disturbance and unmodeled dynamic. In contrast to [44–46,48], the proposal considers the estimation error originally proposed by [41–43].
2. **Implementing a SISO CAPBC angular speed control.** The proposed technique is applied to the outer loop of an IFOC for IMs, where it controls the angular speed. Implementing the CAPBC is more complex than the DAPBC from [27] but improves performance by incorporating online parameter adaptive estimation. The controller does not require knowledge of the motor load mechanical parameters, unlike the PIC.
3. **Implementing a MIMO CAPBC d-q axis current control.** The proposed technique is also applied to the inner loop of an IFOC for IMs, where it controls the stator current vector components. In contrast to previous works [44–46,48], the CAPBC can handle systems with an utterly unknown B with a known control direction (KCD), which is the case for IMs.

Moreover, this paper presents experimental results that compare the proposed CAPBC, DAPBC, and PIC techniques in an IFOC scheme for IMs. These tests include more changes than the ones considered in previous studies [27,39,40]. Specifically, the tests consider changes in angular speed reference, parameters that affect field orientation, and load torque. The results demonstrate that the proposed technique is effective and outperforms DAPBC and PIC techniques.

This paper has five sections. The first section is the introduction. Section 2 explains the IM dynamical model and the IFOC control scheme for IMs. This section also provides detailed information on the PIC adjustments and CMRAC basis. Section 3 proposes the CAPBC method for a specific type of nonlinear system that includes IMs. In addition, the authors provide theoretical proof of the proposed method. Section 4 depicts comparative experimental results with PIC and DAPBC, showing the effectiveness and robustness of CMRAC. This section also includes a discussion of the results. Lastly, Section 5 concludes the findings of this paper.

2. Preliminaries

2.1. d-q IM Dynamic Model and IFOC Diagram

The IM model considers a two-pole machine whose results can be expanded for more poles. It is assumed that the rotor and stator windings are distributed symmetrically, the signals are sinusoidal (neglecting the harmonic effects), and that hysteresis, iron losses, and saturation are negligible. The machine operates within the linear zone of the magnetic field, and all motor parameters are constant and referred to the stator. Moreover, a quadrature-phase machine with a smooth air gap is considered [49] (Section 2.1.5). Kirchhoff laws for the stator and rotor circuit are applied [49], and the Park transformation [50] is used to shift the electrical equations to a rotating synchronous reference frame. The vectors are then split into real and imaginary parts, and the IM d-q model used by the FOC scheme is obtained. This is combined with the motion equation obtained from the second Newton law for rotational motion, resulting in the following [49] (Section 2.8):

$$\dot{I}_{sd} = -\frac{R'_s}{\sigma L_s}I_{sd} + \omega_e I_{sq} + \frac{R_r L_m}{\sigma L_s L_r^2}\Psi_{rd} - \frac{L_m}{\sigma L_s L_r}\frac{p}{2}\omega_r \Psi_{rq} + \frac{1}{\sigma L_s}V_{sd},$$

$$\dot{I}_{sq} = -\frac{R'_s}{\sigma L_s}I_{sq} - \omega_e I_{sd} + \frac{R_r L_m}{\sigma L_s L_r^2}\Psi_{rq} + \frac{L_m}{\sigma L_s L_r}\frac{p}{2}\omega_r \Psi_{rd} + \frac{1}{\sigma L_s}V_{sq},$$

$$\dot{\Psi}_{rd} = -\frac{R_r}{L_r}\Psi_{rd} + \left(\omega_e - \frac{p}{2}\omega_r\right)\Psi_{rq} + \frac{R_r L_m}{L_r}I_{sd}, \tag{1}$$

$$\dot{\Psi}_{rq} = -\frac{R_r}{L_r}\Psi_{rq} - \left(\omega_e - \frac{p}{2}\omega_r\right)\Psi_{rd} + \frac{R_r L_m}{L_r}I_{sq},$$

$$\dot{\omega}_r = -\frac{B_p}{J}\omega_r - \frac{1}{J}(T_e - T_l), \text{ with } T_e = \frac{3}{2}\frac{p}{2}\frac{L_m}{L_r}\left(\Psi_{rd}I_{sq} - \Psi_{rq}I_{sd}\right).$$

Here, the variables are the amplitude of the sinusoidal signals at the motor terminals expressed as the direct and quadrature stator current amplitudes I_{sd}, I_{sq}, the direct and quadrature stator voltage amplitudes V_{sd}, V_{sq}, and the direct and quadrature rotor flux amplitudes Ψ_{rd} and Ψ_{rq}. ω_r is the rotor angular speed at the shaft, ω_e is the angular electrical frequency or speed of the synchronous reference frame, T_e is the electromagnetic motor output torque, and T_l is the load torque. The parameters R_s, R_r are the stator and rotor resistances of a phase winding, p are the poles number, J is the motor load inertia, B_p is the viscous coefficient, L_s, L_r, and L_m are the stator, rotor, and magnetizing inductances, respectively, $\sigma = 1 - \frac{L_m^2}{L_r L_s}$ is the dispersion coefficient, and $R'_s = R_s + \frac{L_m^2 R_r}{L_r^2}$ is the stator transient resistance. Finally, the model uses the following first-time derivatives: $\dot{I}_{sd} = \frac{dI_{sd}}{dt}$, $\dot{I}_{sq} = \frac{dI_{sq}}{dt}$, $\dot{\Psi}_{sd} = \frac{d\Psi_{sd}}{dt}$, $\dot{\Psi}_{sq} = \frac{d\Psi_{sq}}{dt}$, and $\dot{\omega}_r = \frac{d\omega_r}{dt}$.

Remark 1. *The coupling between electromagnetic torque, stator current, and rotor flux can be observed in Equation* (1). *As a solution, the IFOC is then achieved for the IM d-q model* (1) *after imposing the following electrical angular frequency (please see details in Appendix A) and operating with a fixed* I^*_{sd} [5] *(Section 4.1):*

$$\omega_e = \frac{p}{2}\omega_r + \alpha \frac{1}{\hat{\tau}_r}\frac{I^*_{sq}}{I^*_{sd}}. \tag{2}$$

Here, I^*_{sd}, I^*_{sq} are the required direct and quadrature stator current amplitudes. $\hat{\tau}_r$ is the estimated rotor time constant, and $\alpha = 1$.

As a result of applying the electrical angular frequency (2), *the quadrature component of the rotor flux tends to zero* $\Psi_{rq} \to 0$. *Thus,* $\Psi_{rd} \to L_m I_{sd}$, *and the electromagnetic torque* $T_e \to K_{T_e} I_{sq}$, *with a constant* $K_{T_e} = \frac{3}{2}\frac{p}{2}\frac{L_m^2}{L_r}I_{sd}$. *Therefore, the following simplified IM d-q model is obtained* [49] *(Section 2.8):*

$$\dot{I}_{sd} = -\frac{R'_s}{\sigma L_s}I_{sd} + \left(\omega_e I_{sq} + \frac{R_r L_m^2}{\sigma L_s L_r^2}I_{sd}\right) + \frac{1}{\sigma L_s}V_{sd},$$

$$\dot{I}_{sq} = -\frac{R'_s}{\sigma L_s}I_{sq} + \left(-\omega_e I_{sd} + \frac{L_m^2}{\sigma L_s L_r}\frac{p}{2}\omega_r I_{sd}\right) + \frac{1}{\sigma L_s}V_{sq}, \tag{3}$$

$$\dot{\omega}_r = -\frac{B_p}{J}\omega_r - K_{T_e}I_{sq} + \left(\frac{1}{J}T_l\right).$$

This simplified d-q model considers I_{sq} *as an electromagnetic torque-producing current and* I_{sd} *as a rotor-flux-producing current. Then,* I_{sd} *is controlled to achieve constant rotor flux control, and* I_{sq} *is used to control the electromagnetic torque for the load demands at different rotor speeds. This way, torque and flux can be controlled independently, similar to DC machines that are separately excited, which is the aim of the IFOC* (3). *Figure 1 depicts the IFOC block diagram.*

Remark 2. *The simplified d-q model* (3) *has the nonlinear terms* $\omega_e I_{sd}$, $\omega_e I_{sq}$, *and* $\omega_r I_{sd}$. *Moreover, the load torque term* T_l *is often considered as a disturbance.*

The following section describes the adjustment of the basic PIC considered for rotor angular speed and stator current vector of the IFOC for IMs. This controller assumes the operation at a fixed angular rotor speed. Thus, ω_e and ω_r are constant, and model (3)

behaves as an LDS. Furthermore, the outer loop PIC neglects the T_l disturbance and expects robustness in front of its variations.
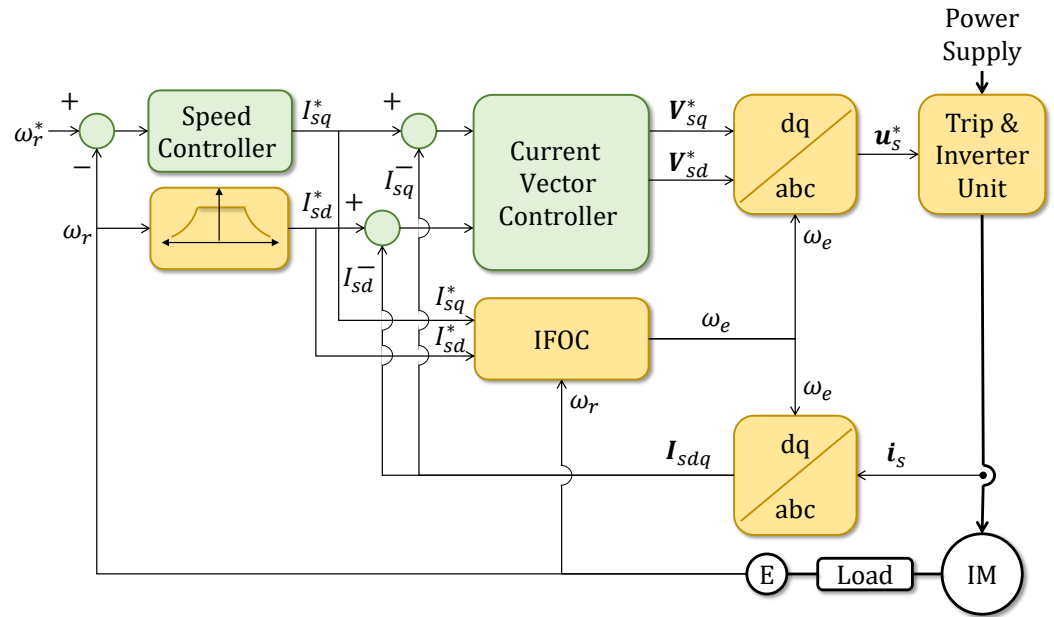
Figure 1. IFOC diagram for IMs based on [5] (Section 4.1).

2.2. PIC Adjustment

Appendix B describes the PIC adjustment theory in detail. As a summary, the inner current controllers' parameters are computed as follows (based on [9]):

$$V_{sq}^* = \left(K_{Pi}e_{I_{sq}} + K_{Ii} \int e_{I_{sq}}d\tau \right) \text{ and } V_{sd}^* = \left(K_{Pi}e_{I_{sd}} + K_{Ii} \int e_{I_{sd}}d\tau \right)$$

$$\text{where } K_{Ii} = \frac{R_s'\tau_i\omega_{ni}^2}{H_oH_i} \text{ and } K_{Pi} = \frac{R_s'(\tau_i2\xi_i\omega_{ni} - 1)}{H_oH_i}. \tag{4}$$

Here, V_{sq}^* and V_{sd}^* are the direct and quadrature stator voltage references, K_{Pi} and K_{Ii} are the PICs inner proportional and integral parameters, $e_{I_{sq}}$ and $e_{I_{sd}}$ are the direct and quadrature stator current errors, τ_i is the electrical time-constant, H_o is the inverter gain, and H_i is the current sensor gain.

As design criteria, a root locus method is often applied. The inner damping coefficient value ξ_i is chosen between 0.5 and 0.8, with the most common value for this application considering $\xi_i = \frac{\sqrt{2}}{2} \approx 0.707$. The inner natural frequency equals $\omega_{ni} = \frac{2.3}{\tau_i}$ [51], which in this AC drive case should be higher than the switching frequency of the inverter´s IGBTs, having a value between 1.7 kHz and 16 kHz for powers between 1500 kW and 37 kW, respectively [52].

Moreover, the outer angular speed controllers' parameters are computed as follows (based on [9]):

$$I_{sq}^* = \left(K_{Po}e_{\omega_r} + K_{Io} \int e_{\omega_r}d\tau \right) K_{T_e}^{-1}$$

$$\text{where } K_{Io} = \frac{H_iB_p\tau_o\omega_{no}^2}{H_o} \text{ and } K_{Po} = \frac{H_iB_p(2\xi_o\omega_{no}\tau_o - 1)}{H_o}, \tag{5}$$

where I_{sq}^* is the quadrature stator current set point, K_{Po} and K_{Io} are the PICs outer proportional and integral parameters, e_{ω_r} is the rotor angular speed error, τ_o is the mechanical time-constant, and H_o is the speed sensor gain. Here, the squared outer natural frequency is $\omega_{no}^2 = (K_{Io}H_o)/(H_iB_p\tau_o)$, which is used to obtain the fixed-gain parameter K_{Io} of the

controller after considering $\omega_{no} = \frac{\omega_{ni}}{15}$ [51,53]. The term depending on the outer natural frequency ω_{no} and the outer damping coefficient ξ_o is $2\xi_o\omega_{no} = (H_iB_p + K_{Po}H_o)/(H_iB_p\tau_o)$, and it is used to compute the fixed-gain parameter K_{Po} of the controller.

Remark 3. *Please observe that PIC adjustment depends on the knowledge of the plant parameter values. Here, the resistances vary with the motor temperature, for instance. Therefore, using an adaptive controller would assure robustness regarding parameter variations.*

The following section describes the CMRAC basis this manuscript considers when proposing CAPBC.

2.3. CMRAC Basis to Be Expanded for CAPBC

The CMRAC applies to scalar LDS, with relative degree 1 of the following form:

$$\dot{y}(t) = ay(t) + bu(t). \tag{6}$$

Here, the plant parameters a and $b \in \Re$ are constant and unknown, with known $sign(b)$. The LDS's input and output are $u(t)$ and $y(t) \in \Re$, respectively.

The CMRAC is associated with the following equations [41]:

$$\dot{y}_r(t) = -k_c y_r(t) + b_r y^*(t), \quad \text{Reference model} \tag{7}$$

$$\dot{\hat{y}}(t) = -k_i e_i + \hat{\theta}_i^T \omega_i, \quad \text{Identification model} \tag{8}$$

$$u(t) = \hat{\theta}_c^T \omega_c, \quad \text{Control law} \tag{9}$$

$$\left.\begin{array}{l} \dot{\hat{\theta}}_1(t) = sign(b)(e_c(t)y(t) + \varepsilon_1(t)), \\ \dot{\hat{\theta}}_2(t) = sign(b)(e_c(t)y_r(t) + \varepsilon_2(t)), \end{array}\right\} \quad \text{Control adaptive law} \tag{10}$$

$$\left.\begin{array}{l} \varepsilon_1(t) = -(\hat{a} + k_c) + \hat{b}(t)\hat{\theta}_1(t), \\ \varepsilon_2(t) = -b_r + \hat{b}(t)\hat{\theta}_2(t), \end{array}\right\} \quad \text{Closed-loop estimation error} \tag{11}$$

$$\left.\begin{array}{l} \dot{\hat{a}}(t) = -(e_i(t)y(t) - \varepsilon_1(t)), \\ \dot{\hat{b}}(t) = -(e_i(t)u(t) - \varepsilon_1(t)\hat{\theta}_1(t) - \varepsilon_2(t)\hat{\theta}_2(t)). \end{array}\right\} \quad \text{Identification adaptive law} \tag{12}$$

Here, the variable $y_r(t) \in \Re$ is the reference model output and $\hat{y}(t) \in \Re$ is the identification model output. The bounded reference trajectory is $y^*(t) \in \Re$. Furthermore, $e_c = (y_r(t) - y(t)) \in \Re$ and $e_i(t) = (\hat{y}(t) - y(t)) \in \Re$ are the control and identification errors. The adaptive parameters for control are $\hat{\theta}_c(t)$, and for identification, $\hat{\theta}_i(t) \in \Re^2$. The designer chooses the model parameters $b_r, k_c \in \Re^+$, and $k_i \in \Re$, and $\omega_c, \omega_i \in \Re^2$ are the control and identification vector information. The estimated controller parameter $\hat{\theta}_c^T = \begin{bmatrix} \hat{\theta}_1 & \hat{\theta}_2 \end{bmatrix}$, and the estimated plant parameter $\hat{\theta}_i^T = \begin{bmatrix} \hat{a} & \hat{b} \end{bmatrix}$. Finally, the ideal controller parameters $\theta_1, \theta_2 \in \Re$ fulfill the following condition:

$$-(a + k_c) + b\theta_1 = 0 \text{ and } -b_r + b\theta_2 = 0. \tag{13}$$

Once this CMRAC is applied to system (6) and it is assumed that $b = |b|sign(b)$, the obtained closed-loop autonomous system ensures that $e_c(t)$, $e_i(t)$, $\varepsilon_1(t)$, and $\varepsilon_2(t)$ tend asymptotically to zero.

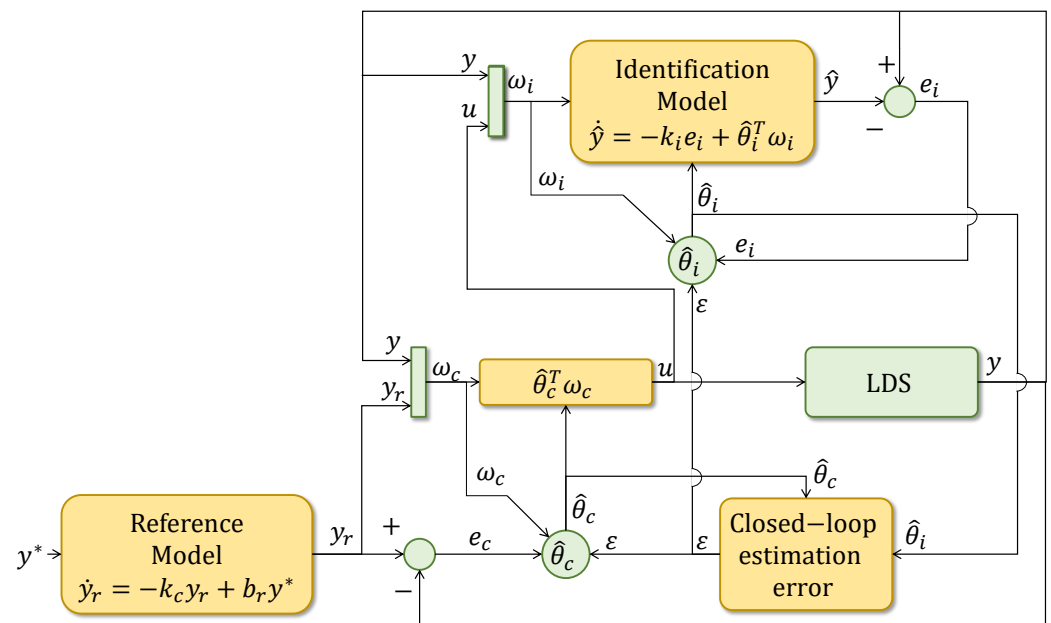Figure 2 shows the CMRAC control diagram for LDS dynamical systems.

Figure 2. CMRAC diagram based on [41].

Remark 4. *The C approach enhances the D and I approaches by taking into account the closed-loop estimation error. However, it does not apply to NLDS with disturbances and unmodeled dynamics. Furthermore, CMRAC has had tuning issues for Kc and Ki, which have recently been resolved [27].*

Based on the previous background and as a solution to the described issues, the following section proposes a robust CAPBC for MIMO NLDS.
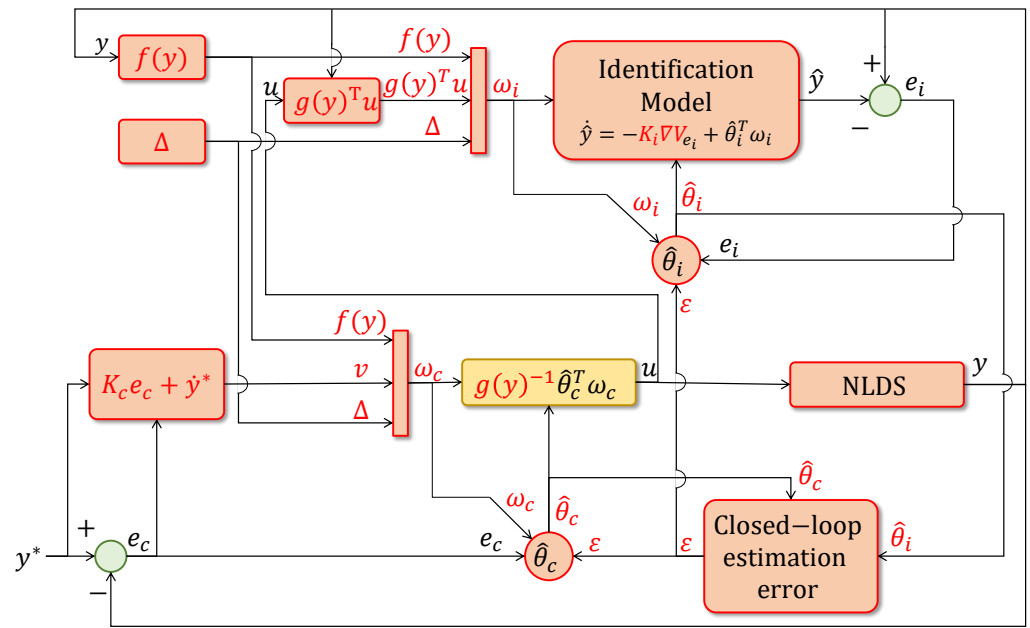
3. Proposed CAPBC

This section outlines the proposed CAPBC, which combines the D and I approaches, considering the closed-loop estimation error of the adaptive parameters based on the CMRAC ideas [41–43] described in Section 2.3. Additionally, the proposal is adaptive and does not rely on explicit knowledge of the plant parameters, as in the case of PIC described in Section 2.2. However, this CAPBC has specific tuning formulas similar to the PIC, but depending on the known plant operational expansion the DAPBC [27], and applies to both LDS and NLDS with disturbances and unmodeled dynamics. Consequently, the proposal solves the issues described in Remark 4 of CMRAC.

Figure 3 illustrates the proposed CAPBC diagram, which is then applied to the inner and outer control loops of the IFOC diagram described in Section 2.1 for IMs.

The proposed CAPBC shown in Figure 3 lacks of a reference model [41] and applies to MIMO dynamical systems of the following form:

$$\dot{y}(t) = A^T f(y) + B^T g(y)^T u + \delta^T \Delta + \zeta. \tag{14}$$

Here, the output $y(t) \in \mathfrak{R}^n$ and the input $u(t) \in \mathfrak{R}^n$ are accessible. The functions $g(y) \in \mathfrak{R}^{nxn}$, and $f(y) \in \mathfrak{R}^m$ are known, like the disturbance portion $\Delta \in \mathfrak{R}^n$. The unmodeled dynamics $\zeta \in \mathfrak{R}^n$ are unknown, as well as the plant parameters $A^T \in \mathfrak{R}^{nxm}$, $B^T, \delta^T \in \mathfrak{R}^{nxn}$.

Figure 3. Proposed CAPBC diagram for MIMO NLDS; the differences are marked in red.

The following theorem details the proposal for the class of NLDS (14):

Theorem 1. *The following CAPBC assures the output $y(t) \in \mathfrak{R}^n$ of NLDS (14) tracks the reference $y^*(t) \in \mathfrak{R}^n$ while observing it via $\hat{y}(t) \in \mathfrak{R}^n$:*

$$\dot{\hat{y}}(t) = -K_i \nabla V_{e_i}(t)^T + \hat{\theta}_i^T \omega_i, \qquad \text{Identification model} \qquad (15)$$

$$u(t) = g(y)^{-1} \hat{\theta}_c^T \omega_c, \qquad \text{Control law} \qquad (16)$$

$$\dot{\hat{\theta}}_c^T = \left(S^T \nabla V_{e_c} \omega_c^T - S^T \varepsilon^T \Gamma_\varepsilon^{-1} + \sigma_c \hat{\theta}_c^T \right) \Gamma_c, \qquad \text{Control adaptive law} \qquad (17)$$

$$\varepsilon = \begin{bmatrix} \varepsilon_1 \\ \varepsilon_2 \\ \varepsilon_3 \end{bmatrix} = \begin{bmatrix} \hat{B}^T \hat{\theta}_1^T + \hat{A}^T \\ \hat{B}^T \hat{\theta}_2^T - I_n \\ \hat{B}^T \hat{\theta}_3^T + \hat{\delta}^T \end{bmatrix}, \qquad \text{Closed-loop estimation error} \qquad (18)$$

$$\dot{\hat{\theta}}_i^T = \left(\omega_i^T \nabla V_{e_i} - \varepsilon^T \Gamma_\varepsilon^{-1} (P_1^T + \hat{\theta}_c P_2^T) + \sigma_i \hat{\theta}_i^T \right) \Gamma_i, \qquad \text{Identification adaptive law} \qquad (19)$$

Here, $\nabla V_{e_c} \in \mathfrak{R}^{1 \times n}$ and $\nabla V_{e_i} \in \mathfrak{R}^{1 \times n}$ are the gradients of the design Lyapunov-type energy functions V_{e_c} and V_{e_i}. The control and identification errors are $e_c(t) = y^*(t) - y(t)$ and $e_i(t) = y(t) - \hat{y}(t)$, with $e_c(t), e_i(t) \in \mathfrak{R}^n$. The adaptive controller and identification parameters are $\hat{\theta}_c^T$ and $\hat{\theta}_i^T(t) \in \mathfrak{R}^{n \times (2n+m)}$, depending on the control and identification adaptive law modifications σ_c and $\sigma_i \in \mathfrak{R}^{n \times n}$, which are positive-definite. The information vectors for control and identification are ω_c and $\omega_i \in R^{(2n+m) \times 1}$, where $\omega_c^T = \begin{bmatrix} f(y)^T & (K_c e_c + \dot{y}^*)^T & \Delta^T \end{bmatrix}^T$ and $\omega_i^T = \begin{bmatrix} f(y)^T & (g(y)^T u)^T & \Delta^T \end{bmatrix}^T$. The auxiliary known parameters $P_1 = \begin{bmatrix} I_m & 0 & 0 \\ 0 & 0_n & 0 \\ 0 & 0 & I_n \end{bmatrix}$ and $P_2 = \begin{bmatrix} 0_m & I_n & 0_n \end{bmatrix}$, where I_m and I_n are identity matrices of order m and n, respectively. Moreover, 0_n and 0_m are null matrices of order n and m, respectively. The estimated plant parameter $\hat{\theta}_i^T = \begin{bmatrix} \hat{A}^T & \hat{B}^T & \hat{\delta}^T \end{bmatrix}$ (19) finds $\hat{A} \in R^{n \times m}$, $\hat{B}$, and $\hat{\delta} \in R^{n \times n}$. The estimated controller parameter $\hat{\theta}_c^T = \begin{bmatrix} \hat{\theta}_1^T & \hat{\theta}_2^T & \hat{\theta}_3^T \end{bmatrix}$ (17), computes $\hat{\theta}_1 \in R^{n \times m}$, $\hat{\theta}_2$, and $\hat{\theta}_3 \in R^{n \times n}$. Later, these results allow implementing the closed-loop estimation error (18).

The designer adjusts the control and identification gains Γ_c, Γ_i, and $\Gamma_\varepsilon \in \mathfrak{R}^{(2n+m) \times (2n+m)}$, where $\Gamma_c = \Gamma_\varepsilon = \left(\frac{\mu_c}{1 + \omega_{cn}^T \omega_{cn}} \right)$, $\Gamma_i = \left(\frac{\mu_i}{1 + \omega_{in}^T \omega_{in}} \right)$, where ω_{cn} and ω_{in} are the vectors containing the upper operational range of each element of ω_c and ω_i. Also, it adjusts the forgetting factors

$\mu_c \in \mathfrak{R}^+$ *and* $\mu_i \in \mathfrak{R}^+$ *[54]—(Section 4.3.6) and (Remark 4.3.7). Furthermore, the designer adjusts controller parameters* K_c *and* $K_i \in \mathfrak{R}^{nxn}$*. The ideal control and identification parameters are* θ_c^T *and* $\theta_i^T \in \mathfrak{R}^{nx(2n+m)}$*, which are defined as follows:*

$$\theta_i^T = \begin{bmatrix} A^T & B^T & \delta^T \end{bmatrix} \tag{20}$$

$$B^T \theta_1^T + A^T = 0 \, , \, B^T \theta_2^T - I_n = 0 \text{ and } B^T \theta_3^T + \delta^T = 0. \tag{21}$$

The error of the parameters are $\Phi_c^T = \theta_c^T - \hat{\theta}_c^T$ *and* $\Phi_i^T = \theta_i^T - \hat{\theta}_i^T \in R^{nx(2n+m)}$*.*
Appendix C describes the CAPBC stability proof. ◊

The proposed CAPBC is utilized in an IFOC scheme for IMs, as depicted in Figure 4.
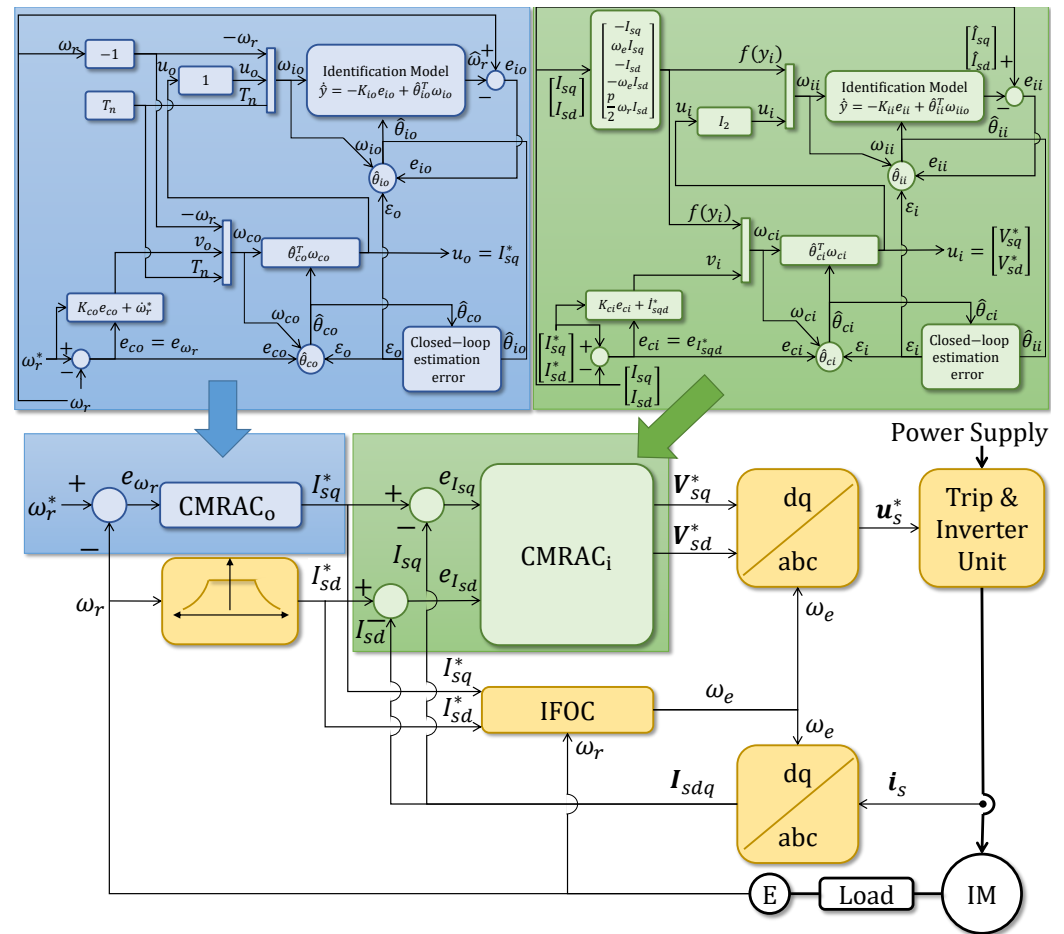
Figure 4. IFOC diagram for IMs with the proposed CAPBCs.

The design considers the simplified IM d-q model (3) and divides it into the electrical and mechanical subsystems to be controlled in cascade. The first two equations of (3) represent the inner-loop electrical subsystem, with an inner output y_i of the form $y_i = \begin{bmatrix} I_{sq} & I_{sd} \end{bmatrix}^T$ and an inner control input u_i of the form $u_i = \begin{bmatrix} V_{sq}^* & V_{sd}^* \end{bmatrix}^T$. On the other hand, the last equation of (3) represents the outer-loop mechanical subsystem, with an outer output y_o of the form $y_o = \omega_r$ and an outer control input u_o of the form $u_o = I_{sq}^*$.

The design of the outer loop controller $CAPBC_o$ considers the known disturbance portion Δ to be equal to the nominal torque T_n, and there is no disturbance for the inner loop. The function $g(y)$ is equal to 1, and $f(y)$ is equal to $-\omega_r$. Moreover. the design of the inner controller $CAPBC_i$ assumes there is no disturbance and that there are unmodelled dynamics of the inverter. The function $g(y)$ is equal to the identity matrix of order two I_2, and $f(y)$ is equal to $\begin{bmatrix} -I_{sq} & \omega_e I_{sq} & -I_{sd} & -\omega_e I_{sd} & \frac{p}{2}\omega_r I_{sd} \end{bmatrix}^T$.

The design Lyapunov-type energy functions are $V_{e_{co}} = e_{oc}^2/2$ and $V_{e_{io}} = e_{io}^2/2$ for the outer loop, and $V_{e_{ci}} = e_{ci}^T e_{ci}/2$ and $V_{e_{ii}} = e_{ii}^T e_{ii}/2$ for the inner loop. Therefore, their respective gradients are $\nabla V_{e_{co}} = e_{oc}$, $\nabla V_{e_{io}} = e_{io}$, $\nabla V_{e_{ci}} = e_{ci}^T$, and $\nabla V_{e_{ii}} = e_{ii}^T$.

The following section discusses the obtained comparative experimental results.

4. Experimental Results

Figure 5 shows the pictures of the test bench used to validate the proposal, joined with its control diagram.
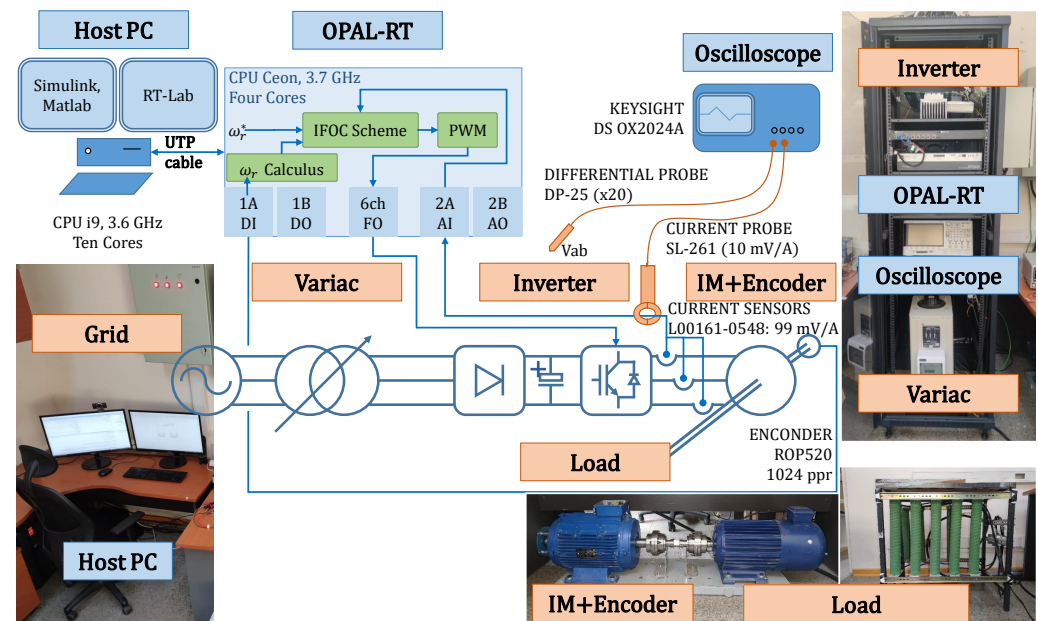
Figure 5. Test bench pictures and control diagram.

It has a real-time simulator controller OPAL-RT 4510 v2 from OPAL-RT Technologies, Montréal, QC, Canada that inherently uses a bipolar pulse width modulation (PWM), switching at 8 kHz. It commands a two-level voltage source inverter that feeds an IM-load assembly, sending the trip pulses via fiber optic (FO) cables. Simulink version 10.4 of Matlab R2021b (9.11.0.1769968) for Win64 running on a Host PC allows building the IFOC scheme of Figure 1 using PIC, DAPBC, and the proposed CAPBC and downloading them to the control platform using the software RT-LAB v2020.2.2.82. The motor data plate has 7500 kW, 380 V, 50 Hz, 1455 rpm, $fp = 0.85$, and two pairs of poles $p = 2$. A rotor time constant of $\tau_r = 0.221$ was used to implement FOC (2), which is taken from previous measurements ([16], Tables IV, Motor II).

The following controllers were programmed into the IFOC scheme:

1. **PIC** (4) **and** (5). These controllers were adjusted as described in Section 2.2 and using the motor load parameter values from [16] (Tables III, IM 2) that followed the IEEE standard 112A, including DC injection, locked rotor, and free load [13] (Section 5.9).
2. **DAPBC [27] (Theorem 1)** It uses both a SISO controller $I_{sq}^* = \hat{\theta}_{oc} \omega_{oc}$ and a MIMO controller $\begin{bmatrix} Vsq^* \\ Vsd^* \end{bmatrix} = \hat{\theta}_{ic} \omega_{ic}$, as in [27] (Equation (4)). The motor load parameter does not need to be known to adjust DAPBC.
3. **Proposed CAPBC from Theorem 1.** It also uses both a SISO controller $I_{sq}^* = \hat{\theta}_{oc} \omega_{oc}$ and a MIMO controller $\begin{bmatrix} Vsq^* \\ Vsd^* \end{bmatrix} = \hat{\theta}_{ic} \omega_{ic}$, as in Figure 4.

The same 10 s duration test applies to the PIC, DAPBC, and proposed CAPBC strategies. It considers that the IM starts with a 66% torque load and applies a step speed command of 25 rad/s, 60 rad/s, 85 rad/s, 120, and 152.36 rad/s, at times 2 s, 2.5 s, 3 s, 3.5 s,

and 4 s, respectively. Later, the load decreases to 40% at 5 s and increases again to 66% at 6 s. Finally, the field disorientation is considered by adjusting the value of α from IFOC (2) to $\alpha = 0.8$ at 7.5 s and increases again to $\alpha = 1.1$ at 9 s, simulating step changes for the rotor time constant.

Figure 6 exhibits the controller's comparative rotor angular speed response. It can be seen that adaptive controllers are more robust against different variations, including load torque and IFOC-impacting parameter variations. All controllers track the reference speed. However, adaptive controllers exhibit lower maximum overshoot (MO) and faster response than PIC in all scenarios. Here, the proposed CAPBC has the lowest MO and the fastest response. The effectiveness of the proposed CAPBC is superior for the different step changes in the reference speed occurring every 2.5 s until 4 s, as well as for the torque and IFOC variations. The CAPBC enhanced the transient response of the PIC and the DAPBC, as expected.
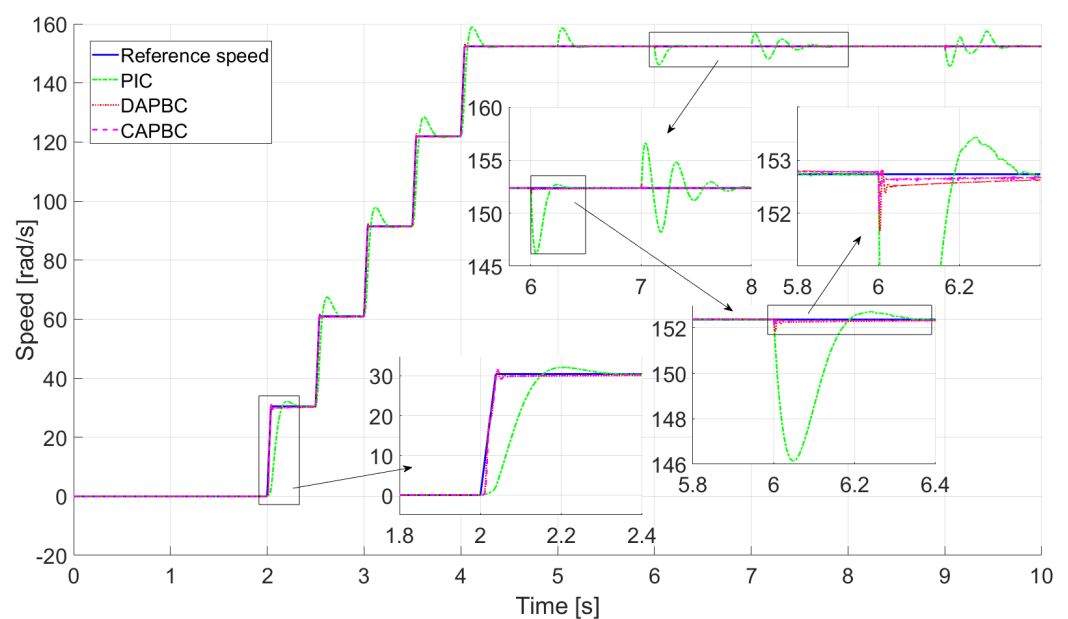

Figure 6. Comparative rotor angular speed.

Table 1 shows comparative performance indexes with more detail than Figure 6.

The CMRAC exhibits the best performance in all scenarios despite having similar steady-state errors (E_{ss}) across the different controllers. The proposal demonstrates the lowest control effort (please see the ISI index) and better transient behavior with the lowest MO and IAE indexes. The performance of the PIC deteriorates significantly when field disorientation occurs at seven and nine seconds with α equal to 0.8 and 1.1, respectively. The proposed CAPBC and DAPBC for the inner loop ensure robustness under this situation due to their MIMO, adaptive natures, and NLDS designs.

Figures 7–9 show the consumed and reference q-axis current for torque production for the PIC, DPABC, and CAPBC, respectively. All controllers track the reference current I_{sq}^* that produces torque, with CMRAC and DAPBC having a faster response than PIC. The PIC has difficulties tracking the reference after nine seconds when field disorientation occurs, as seen in the center-right side of Figure 7. This provokes the tracking difficulties shown in the upper-right side of Figure 6 for the slower speed control outer loop.

Table 1. Comparative performance indexes for the rotor speed controllers.

|		Tests								
	Time [s]	2.0	2.5	3.0	3.5	4.0	5.0	6.0	7.0	9.0
Performance Index	α	1.00	1.00	1.00	1.00	1.00	1.00	1.00	0.80	1.10
	T_l [% T_n]	66.0	66.0	66.0	66.0	66.0	40.0	66.0	66.0	66.0
	Speed [rad/s]	25.0	60.0	85.0	120	152.36	150	152.36	152.36	152.36
Ess [%] (Ending) $\frac{(\omega_r^* - \omega_r)}{\omega_r^*} 100$	PI	0.1299	0.1212	0.1237	0.1189	0.0180	0.0307	0.0254	0.0243	0.0851
	DAPBC	0.0850	0.0302	0.0804	0.0100	0.0063	0.0079	0.0195	0.0227	0.0468
	CAPBC	0.0512	0.0269	0.0659	0.0066	0.0029	0.0068	0.0190	0.0139	0.0171
MO [%] (Starting) $\frac{(\omega_r^* - \omega_r)}{\omega_r^*} 100$	PI	5.5983	10.6929	7.1124	5.3479	4.3302	4.1276	0.2338	2.7979	3.5007
	DAPBC	3.5168	1.7019	1.1308	0.8651	0.7095	0.3595	0.2139	0.1751	0.3143
	CAPBC	3.4904	1.4038	0.8367	0.5941	0.4640	0.2938	0.1923	0.1663	0.1667
IAE [cm.s] $\int |e_{\omega_r}| \, d\tau$	PI	0.6491	0.6494	0.6501	0.6519	0.6541	0.6544	1.043	1.52	2.2654
	DAPBC	0.0152	0.0198	0.0359	0.0368	0.0378	0.0529	0.0663	0.0694	0.1507
	CAPBC	0.0099	0.0059	0.0072	0.0102	0.0223	0.0356	0.0437	0.0452	0.1425
ISI [$\times 10^3$] $\int I_{sq}^{*2} \, d\tau$	PI	0.2785	0.2649	0.2656	0.2664	0.2672	0.3915	0.8797	1.1001	3.3045
	DAPBC	0.2616	0.2619	0.2623	0.2625	0.2632	0.3907	0.8752	0.9837	3.3018
	CAPBC	0.2592	0.2594	0.2610	0.2624	0.2634	0.3900	0.8689	0.9729	3.3016
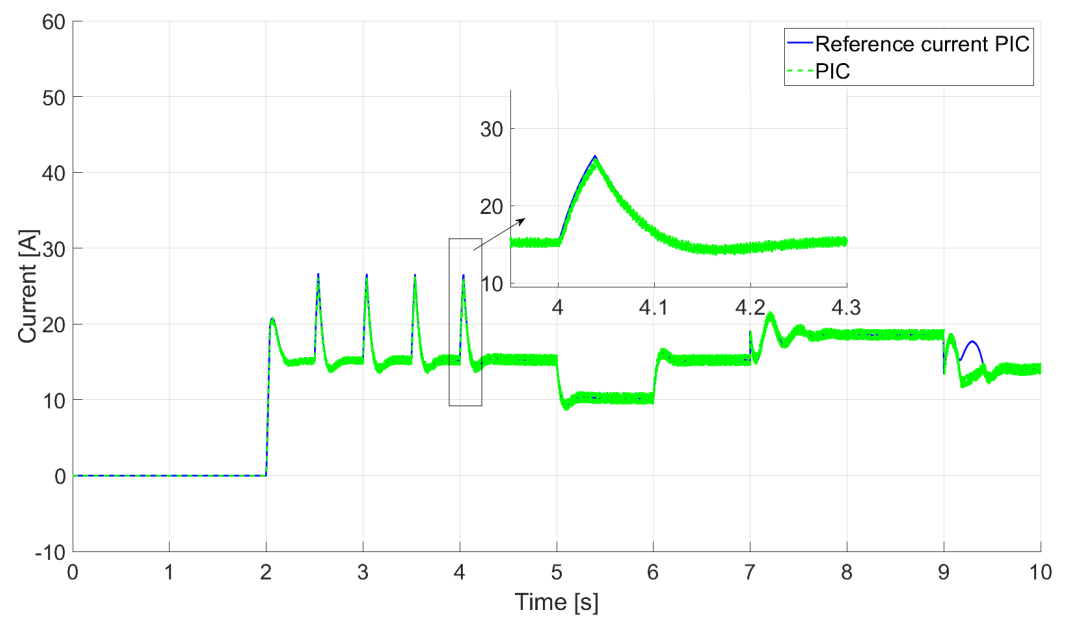
Figure 7. Consumed and reference q-axis current torque producing for PIC.
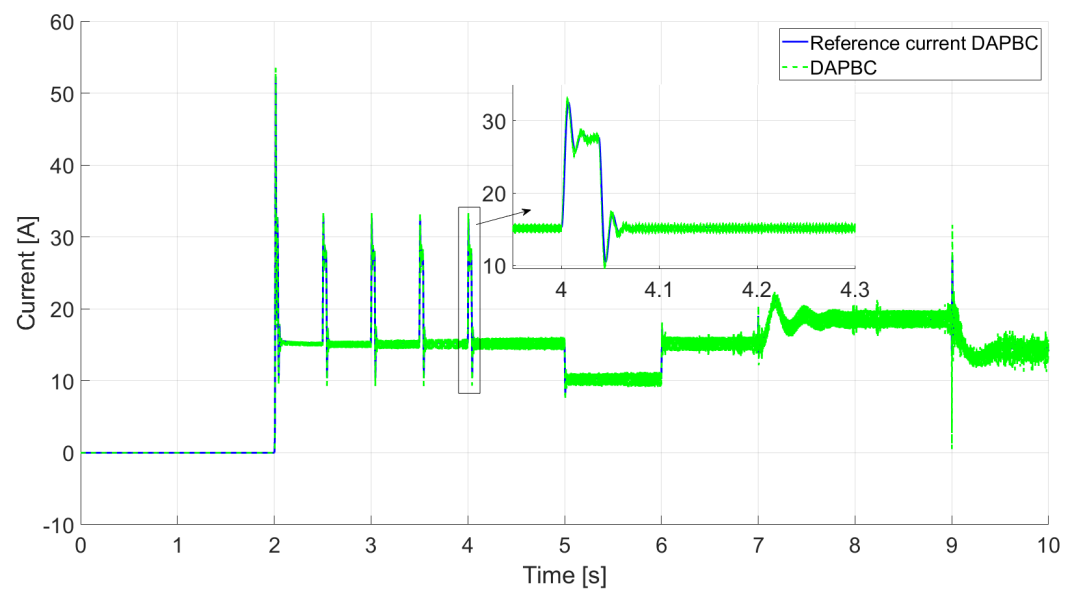
Figure 8. Consumed and reference q-axis current torque producing for DAPBC.
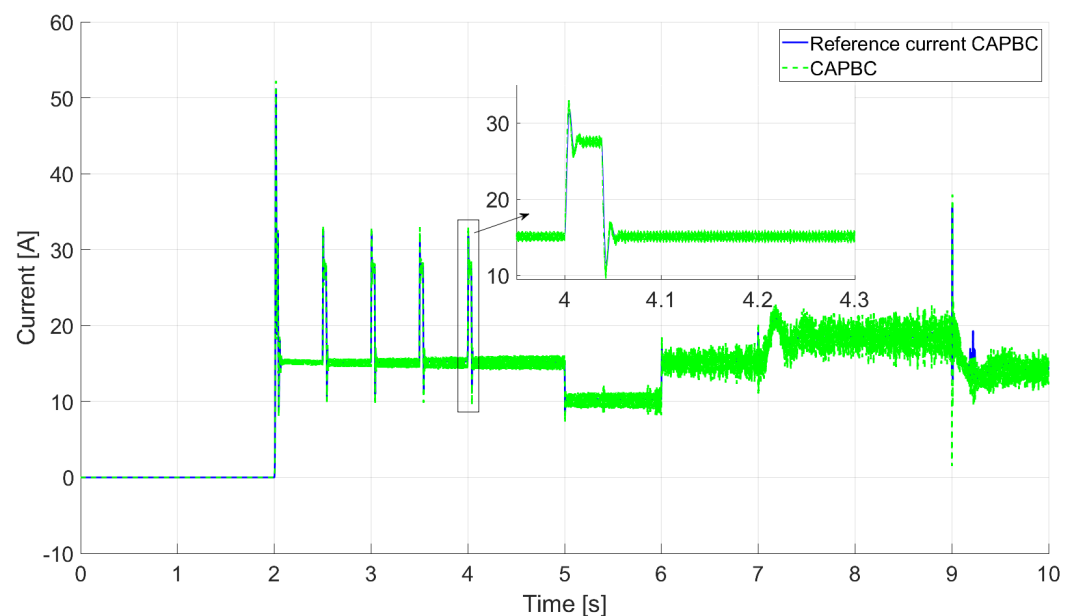
Figure 9. Consumed and reference q-axis current torque producing for the proposed CAPBC.

It can be seen in Figures 7–9 that the faster speed responses of adaptive controllers are achieved with a higher reference and consumed q-axis current torque producing, as expected. Moreover, the line voltages have the typical PWM wayform, with the 50 Hz frequency corresponding to the nominal rotor angular speed, as can be seen in Figures 10–12.

Finally, Figures 10–12 show the oscilloscope line voltage a-b around 6.5 s for the PIC, DPABC, and CAPBC, respectively. In all cases, results show the typical two-level voltage source inverter commended by a bipolar PWM.

DSO-X 2024A, MY58104362 Thu Mar 14 02:35:46 2024
1   10.0A/   2   10.0A/   3   10.0A/   4   150V/   0.0s   3.000 ms/   Stop
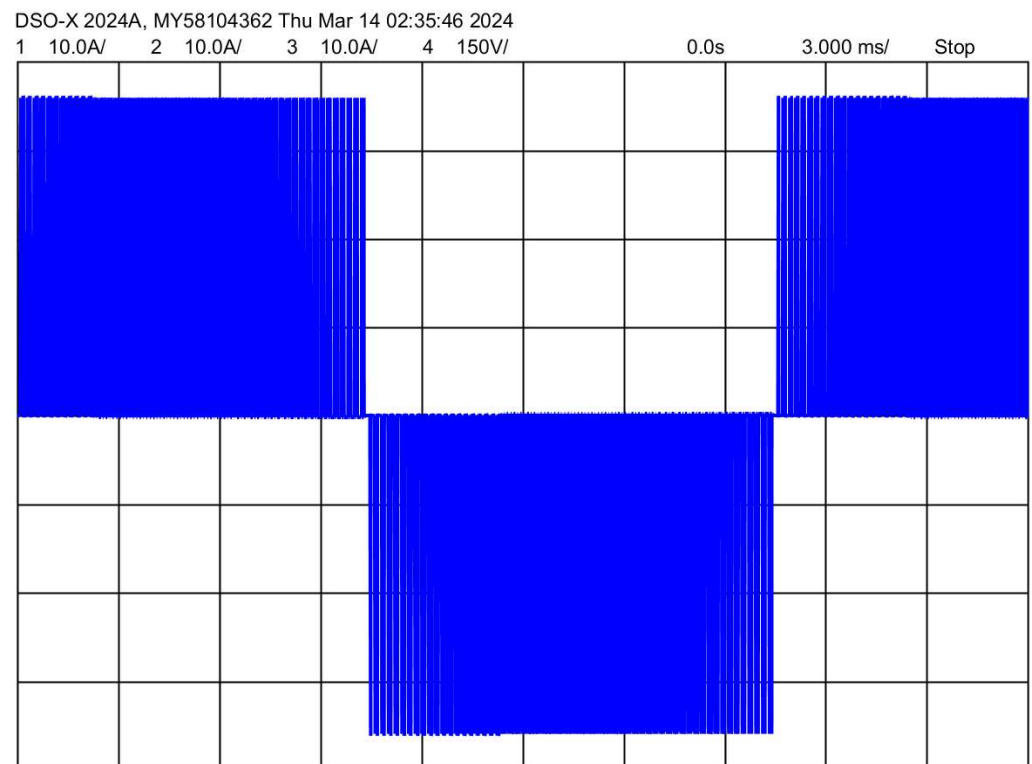
Figure 10. Line voltage a-b around second 6.5 for PIC.

DSO-X 2024A, MY58104362 Thu Mar 14 03:23:32 2024
1   10.0A/   2   10.0A/   3   10.0A/   4   150V/   0.0s   3.000 ms/   Stop
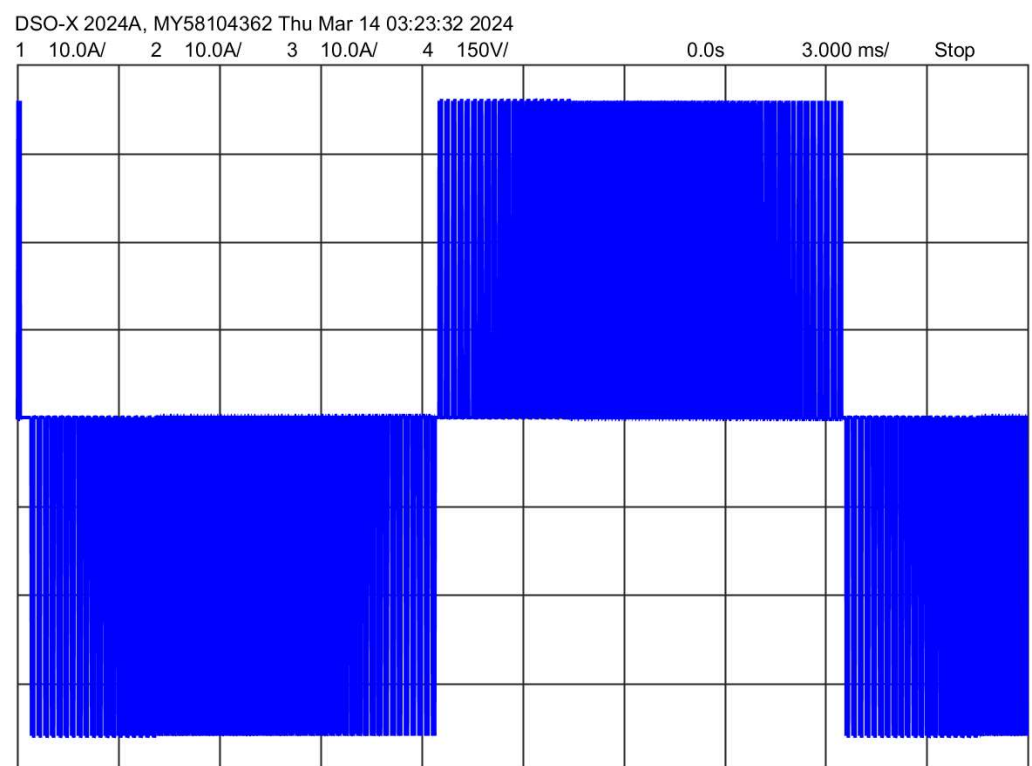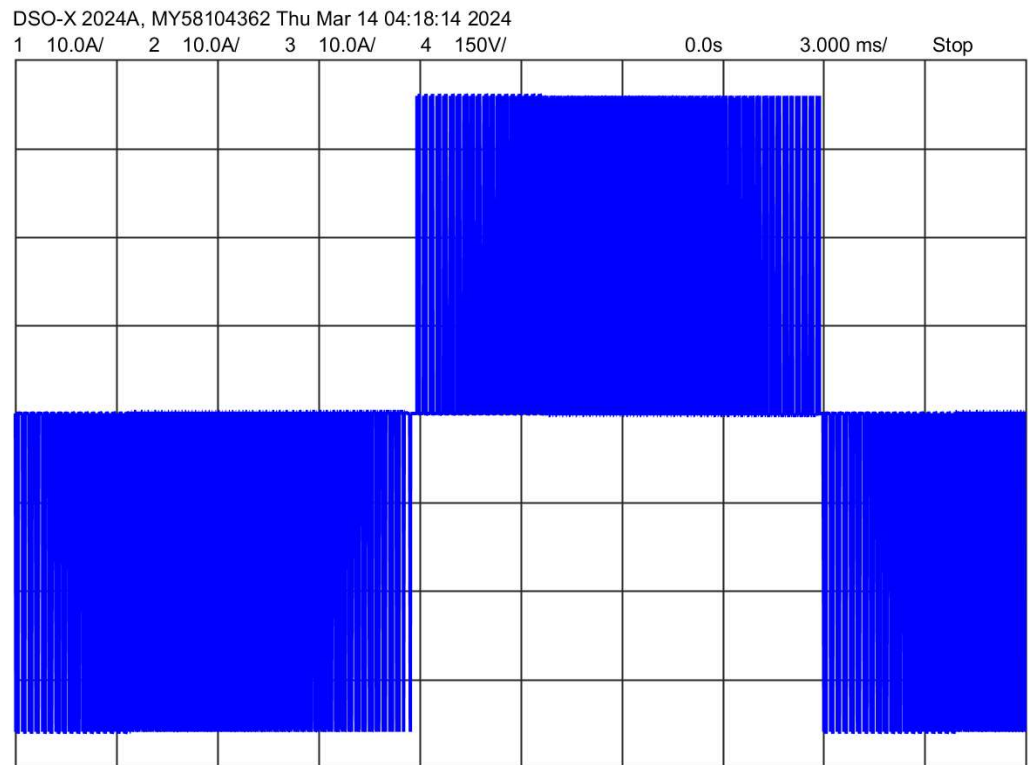
Figure 11. Line voltage a-b around second 6.5 for DAPBC.

Figure 12. Line voltage a-b around second 6.5 for the proposed CAPBC.

5. Conclusions

This paper introduced a novel CAPBC tailored for a class of nonlinear systems encompassing the IMs under an IFOC scheme, including perturbances and unmodeled dynamics. It expands the DAPBC technique [27] based on the combined approach previously proposed for MRAC [41–43]. The theoretical underpinnings of the proposed CAPBC are detailed in Theorem 1, and the stability proof is exhibited in Appendix C.

Later, the proposal implemented a SISO CAPBC angular speed control for the outer loop of an IFOC for IMs in cascade with the inner-loop MIMO CAPBC d-q axis current control. This paper presents comparative experimental results between the proposed CAPBC, the DAPBC, and PIC techniques in an IFOC scheme for an IM of 7.5 kW. The results demonstrate that the proposed technique is effective and outperforms DAPBC and PIC techniques. Unlike traditional PICs, the CAPBC does not need knowledge of the motor load parameters.

Author Contributions: Conceptualization, methodology, writing—original draft preparation, and visualization, J.C.T.-T.; investigation, formal analysis, supervision, project administration, data curation, and resources and funding acquisition, J.C.T.-T., A.J.R.-M. and N.A.-C.; validation, software, and writing—review and editing; A.J.R.-M. and N.A.-C. All authors have read and agreed to the published version of the manuscript.

Data Availability Statement: Data are contained within the article.

Conflicts of Interest: The authors declare no conflicts of interest.

Abbreviations

The following abbreviations are used in this manuscript:

IMs	Induction motors
DC	Direct current
AC	Alternating current
D	Direct approach
I	Indirect approach
C	Combined approach
VSDs	Variable speed drives
FOC	Field-oriented control
VSDs	Variable speed drives
DTC	Direct torque control
IFOC	Indirect field-oriented control
LDS	Linear dynamical systems
NLDS	Nonlinear dynamical systems
PIC	Proportional and integral controller
MRAC	Model reference adaptive control
DMRAC	Direct model reference adaptive control
CMRAC	Combined model reference adaptive control
APBC	Adaptive passivity-based control
DAPBC	Direct adaptive passivity-based control
SMC	Sliding mode control
ANN	Artificial neural network
PSO	Particle swarm optimization technique
SISO	Single-input and single-output
MIMO	Multiple-input and multiple-output
KCD	Known control direction
PWM	Pulse width modulation
Ess [%]	Steady-state error computed as $\frac{(\omega_r^* - \omega_r)}{\omega_r^*} 100$ at the response ending
MO [%]	Maximum overshoot calculated as $\frac{(\omega_r^* - \omega_r)}{\omega_r^*} 100$ at the response starting
IAE [cm.s]	Integral absolute value Error of the output $\int \|e_{\omega_r}\| \, d\tau$
ISI [$\times 10^3$]	Integral squared output $\int I_{sq}^{*2} \, d\tau$

Mathematical Operators

$\dot{x}$	Continuous first-time derivative of x.
$\hat{x}$	Estimated variable or parameter x.
y^*	Set-point or required output variable y.
e, m	Referred to electrical e and mechanical m.
i, o	Inner and outer variable.
y^T	Transpose vector variable y.
$f(y)$, and $g(y)$	Functions of the variable y.

Main Notation

The following main notations are used in this manuscript:

ω_r, ω_e	Rotor and electrical angular speed
θ_r	Rotor position
$\boldsymbol{u}_s$	Stator voltage
$\boldsymbol{i}_s$	Stator current
T_e, T_l, and T_n	Electromagnetic, load, and nominal torque.
p	Number of poles
R_s and R_r	Stator and rotor resistance
L_s' and L_r'	Stator and rotor leakage inductance
L_s, L_r, and L_m	Stator, rotor, and magnetizing inductance
σ	Leakage or coupling coefficient, given by $\sigma = 1 - L_m^2/(L_r L_s)$
R_s'	Stator transient resistance, with $R_s' = R_s + \frac{L_m^2 R_r}{L_r^2}$
τ_σ	Stator transient time constant. Given by $\tau_\sigma = \sigma L_s / R_s'$
τ_r	Rotor time constant $\tau_r = L_r / R_r$
τ_i, and τ_o	Electrical and mechanical time constant
B_p	Mechanical friction factor
J	Moment of inertia
I_{sd}, and I_{sq}	Direct and quadrature stator current amplitudes
V_{sd}, and V_{sq}	Direct and quadrature stator voltage amplitudes
$e_{I_{sq}}$, and $e_{I_{sd}}$	Direct and quadrature stator current errors

e_{ω_r}	Rotor angular speed error
Ψ_{rd}, and Ψ_{rq}	Direct and quadrature rotor flux amplitudes
K_{T_e}	Constant $K_{T_e} = \frac{3}{2}\frac{p}{2}\frac{L_m^2}{L_r}I_{sd}$
K_P and K_I	PICs proportional and integral parameters
H_i, and H_o	Inverter and speed sensor gain
ξ	Damping coefficient
ω_n	Natural frequency
y, and y_r	Plant and reference model output
a, b, A, B, and δ	Plant parameters
b_r, k_c, k_i, K_c, and K_i	Model parameters
e_c, and e_i	Control and identification errors
$\hat{\theta}_c$, and $\hat{\theta}_i$	Adaptive parameters for control and for identification
ω_c, and ω_i	Control and identification vector information
ω_{cn}, and ω_{in}	Vectors containing the upper operational range of each element of ω_c and ω_i
ε	Closed-loop estimation error
Δ	Disturbance portion
ζ	Unmodeled dynamics
∇V_{e_c}, and ∇V_{e_i}	Gradients of the design Lyapunov-type energy functions
σ_c, and σ_i	Positive-definite constants
P_1, and P_2	Auxiliary known parameters
I_m, and I_n	Identity matrix of order m and n
0_m, and 0_n	Null matrix of order m and n
Γ_c, Γ_i and Γ_ε	Control, identification, and closed-loop estimation error gains
μ_c, and μ_i	Forgetting factors

Appendix A. IFOC Method Basis

The basic IFOC method [55] imposes an electrical angular frequency equal to

$$\omega_e = \frac{p}{2}\omega_r + \frac{\hat{L}_m}{\hat{\tau}_r}\frac{I_{sq}}{\hat{\Psi}_{rd}}. \tag{A1}$$

Here, substituting (A1) into the first derivatives of the direct and quadrature rotor flux $\dot{\Psi}_{rd}$ and $\dot{\Psi}_{rq}$ of Equation (1), these rotor fluxes dynamical equations from (1) take the form

$$\dot{\Psi}_{rd} = -\frac{1}{\tau_r}\Psi_{rd} + \frac{\hat{L}_m}{\hat{\tau}_r}\frac{I_{sq}}{\hat{\Psi}_{rq}}\Psi_{rq} + \frac{L_m}{\tau_r}I_{sd},$$

$$\dot{\Psi}_{rq} = -\frac{1}{\tau_r}\Psi_{rq} + \frac{L_m}{\tau_r}\left(1 - \frac{\tau_r\hat{L}_m}{L_m\hat{\tau}_r}\frac{\Psi_{rd}}{\hat{\Psi}_{rd}}\right)I_{sq}. \tag{A2}$$

Then, if the term $\frac{\tau_r\hat{L}_m}{L_m\hat{\tau}_r}\frac{\Psi_{rd}}{\hat{\Psi}_{rd}} = 1$ in this last equation with accurate estimations, the dynamical equation of the quadrature rotor flux component Ψ_{ry} has an exponential behavior tending to zero over time $\Psi_{rq} \to 0$, reaching over the 99% of this final value after five times the rotor-time constant τ_r [9]. Later, $\Psi_{rd} \to L_m I_{sd}$ and the electromagnetic torque $T_e \to \frac{3}{2}\frac{p}{2}\frac{L_m^2}{L_r}I_{sd}I_{sq}$, obtaining the simplified $d-q$ model (3).

However, using Equation (A1) to achieve IFOC needs a flux estimator to obtain $\hat{\Psi}_{rd}$, which is the reason why it is not used in this paper. Therefore, the alternative and more practical method using the electrical angular frequency of Equation (2) is performed in this paper [49,56].

The authors have not found explicit proof of this method in the literature. Thus, we describe it herein. After considering the definition of the rotor time constant $\tau_r = \frac{L_r}{R_r}$ and substituting Equation (2) into the third and fourth equations of (1), the rotor flux dynamical equations from (1) take the form

$$\begin{bmatrix} \dot{\Psi}_{rd} \\ \dot{\Psi}_{rq} \end{bmatrix} = A \begin{bmatrix} \Psi_{rd} \\ \Psi_{rq} \end{bmatrix} + L_m \begin{bmatrix} I_{sd} \\ I_{sq} \end{bmatrix}, \text{ whit } A = \begin{bmatrix} -1 & -\frac{\tau_r}{\hat{\tau}_r} \frac{I^*_{sq}}{I^*_{sd}} \\ \frac{\tau_r}{\hat{\tau}_r} \frac{I^*_{sq}}{I^*_{sd}} & -1 \end{bmatrix}. \tag{A3}$$

After applying the Laplace transform [56] to this last equation, considering constant $\begin{bmatrix} I_{sd} & I_{sq} \end{bmatrix}^T$ and the initial condition $\begin{bmatrix} \Psi_{sd}(0) & \Psi_{sq}(0) \end{bmatrix}^T$, we obtain

$$\begin{bmatrix} \Psi_{rd} \\ \Psi_{rq} \end{bmatrix} = (\tau_r s - A)^{-1} L_m s^{-1} \begin{bmatrix} I_{sd} \\ I_{sq} \end{bmatrix} + (\tau_r s - A)^{-1} \begin{bmatrix} \Psi_{rd}(0) \\ \Psi_{rq}(0) \end{bmatrix}. \tag{A4}$$

Applying the final value theorem [56], where $\lim_{t\to\infty} f(t) = \lim_{s\to 0} sF(s)$, we have

$\lim_{t\to\infty} \begin{bmatrix} \Psi_{sd}(t) & \Psi_{sq}(t) \end{bmatrix}^T = L_m A^{-1} \begin{bmatrix} I_{sd} & I_{sq} \end{bmatrix}^T$. As a result, $\begin{bmatrix} \Psi_{rd} \\ \Psi_{rq} \end{bmatrix} \to L_m \begin{bmatrix} 1 & -\frac{\tau_r}{\hat{\tau}_r} \frac{I^*_{sq}}{I^*_{sd}} \\ \frac{\tau_r}{\hat{\tau}_r} \frac{I^*_{sq}}{I^*_{sd}} & 1 \end{bmatrix} \begin{bmatrix} I_{sd} \\ I_{sq} \end{bmatrix}$.

Then, $\begin{bmatrix} \Psi_{rd} \\ \Psi_{rq} \end{bmatrix} \to \frac{L_m}{\left(1+(\frac{\tau_r I^*_{sq}}{\hat{\tau}_r I^*_{sd}})^2\right)} \begin{bmatrix} I_{sd}\left(1 + \frac{\tau_r I^*_{sq} I_{sq}}{\hat{\tau}_r I^*_{sd} I_{sd}}\right) \\ I_{sq}\left(1 - \frac{\tau_r I^*_{sq} I_{sd}}{\hat{\tau}_r I^*_{sd} I_{sq}}\right) \end{bmatrix}$. Here, if $\frac{\tau_r I^*_{sq} I_{sd}}{\hat{\tau}_r I^*_{sd} I_{sq}} = 1$, we obtain $\begin{bmatrix} \Psi_{rd} \\ \Psi_{rq} \end{bmatrix} \to$

$L_m \begin{bmatrix} I_{sd} \\ 0 \end{bmatrix}$, achieving field orientation. This could be obtained under the presence of accurate parameters estimation, similar to the basic IFOC method, thus $\frac{\tau_r}{\hat{\tau}_r} = 1$; and even if $I_{sd} \neq I^*_{sd}$ and $I_{sq} \neq I^*_{sq}$, but $\frac{I^*_{sq}}{I^*_{sd}} \frac{I_{sd}}{I_{sq}} = 1$, which is a valid case not considered in [56].

Appendix B. PIC Adjustment

The adjustment of the PI controllers starts from the simplified IM d-q model (3) and the IFOC block diagram of Figure 1. These are re-expressed as the transfer function block diagram [53] of Figure A1 in Laplace domain after considering all the motor load parameters and the operating point constant is known.

The inner loop is first adjusted after neglecting the nonlinear terms $\left(\sigma L_s \omega_e I_{sq} + \frac{R_r L^2_m}{L^2_r} I_{sd}\right)$ and $-\left(\sigma L_s \omega_e I_{sd} + \frac{L^2_m}{L_r} \omega_r I_{sd}\right)$. Moreover, it considers the closed-loop transfer functions property of $FT = \frac{G}{1+GH}$ with $H = H_i$ and $G = H_o(K_{Pi} + \frac{K_{Ii}}{s})(\frac{1/R'_s}{\tau_i s+1})$ [53], obtaining the transfer function shown in Figure A1, of the form $FT_i = \frac{\omega^2_n K_{Pi}(s+a)/K_{Ii}H_i}{s^2+2\xi_i\omega_{ni}s+\omega^2_{ni}}$. Here, the squared inner natural frequency $\omega^2_{ni} = \frac{H_o K_{Ii} H_i}{R'_s \tau_i}$ is used to obtain the fixed-gain parameter K_{Ii} of the controller. The term depending on the inner natural frequency ω_{ni} and the inner damping coefficient ξ_i is $2\xi_i\omega_{ni} = \frac{R'_s+H_o K_{Pi}H_i}{R'_s \tau_i}$; and it is used to compute the fixed-gain parameter K_{Pi} of the controller. The inner PICs adjustment results in Equation (4).

Later, it is assumed that the inner loop is stabilized. Therefore, applying the final value theorem [56], where $\lim_{t\to\infty} f(t) = \lim_{s\to 0} sF(s)$, we have that $FT_i \to H_i^{-1}$ and the block diagram of Figure A1 is achieved.

In a similar way to the inner loop, after considering the load torque term $\frac{1}{J} T_c$ as a disturbance that is neglected, and considering the closed-loop transfer functions property, the transfer function $FT_o = \frac{\omega^2_n K_{Po}(s+a)/K_{Io}H_i}{s^2+2\xi_o\omega_{no}s+\omega^2_{no}}$ is obtained [51,53]. Here, the squared outer natural frequency is $\omega^2_{no} = \frac{K_{Io}H_o}{H_i B_p \tau_o}$, and it is used to obtain the fixed-gain parameter K_{Io} of the controller. The term $2\xi_o\omega_{no} = \frac{H_i B_p+K_{Po}H_o}{H_i B_p \tau_o}$, depending on the outer natural frequency and the outer damping coefficient, is used to compute the fixed-gain parameter K_{Po} of the controller. Finally, the outer PIC is adjusted as in Equation (5).

Figure A1. Transfer function block diagram of Basic IFOC for IM.

Figure A2. Transfer function block diagram of basic IFOC for IM once the inner loop is stabilized.

Appendix C. CAPBC Stability Proof

Obtaining the Error Dynamical Equations

Subtracting Equations (14) from (15) and regrouping terms, the following identification error is obtained:

$$\dot{e}_i = -K_i e_i + \Phi_i^T \omega_i + \zeta, \tag{A5}$$

It considers the previously given definitions of $e_i = y - \hat{y}$, θ_i, ω_i. Moreover, the identification parameter error $\Phi_i^T \in R^{nx(2n+m)}$ is defined as $\Phi_i = \theta_i - \hat{\theta}_i$.

Multiplying both sides of the model plant (14) by -1, adding and subtracting the term $K_c e_c + \dot{y}^*$, regrouping and considering previous definitions of $e_c = y^* - y$, θ_c, ω_c, the control error is

$$\dot{e}_c = -K_c e_c + B^T \phi_c^T \omega_c - \zeta, \tag{A6}$$

where $\Phi_c^T \in R^{nx(2n+m)}$.

In contrast to D and I approaches, the C technique considers $\hat{B}^T \hat{\theta}_1^T + \hat{A}^T \neq 0$, $\hat{B}^T \hat{\theta}_2^T - I_n \neq 0$ and $\hat{B}^T \hat{\theta}_3^T + \hat{\delta}^T \neq 0$, obtaining the closed-loop estimation error (18).

Subtracting (18) from (21) (since (21) being equal to zero does not change the equation), to the right side, respectively, and regrouping terms, we obtain

$$
\begin{bmatrix} \varepsilon_1 \\ \varepsilon_2 \\ \varepsilon_3 \end{bmatrix} = \begin{bmatrix} -(B^T - \hat{B}^T)\hat{\theta}_1^T - (A^T - \hat{A}^T) - B^T(\theta_1^T - \hat{\theta}_1^T) \\ -(B^T - \hat{B}^T)\hat{\theta}_2^T - B^T(\theta_2^T - \hat{\theta}_2^T) \\ -(B^T - \hat{B}^T)\hat{\theta}_3^T - (\delta^T - \hat{\delta}^T) - B^T(\theta_3^T - \hat{\theta}_3^T) \end{bmatrix} = \begin{bmatrix} -\Phi_B^T\hat{\theta}_1^T - \Phi_A^T - B^T\Phi_1^T \\ -\Phi_B^T\hat{\theta}_2^T - B^T\Phi_2^T \\ -\Phi_B^T\hat{\theta}_3^T - \Phi_\delta^T - B^T\Phi_3^T \end{bmatrix}.
$$

This result equals

$$
\varepsilon = -\Phi_i^T P_1 - \Phi_i^T P_2 \theta^T - B^T \Phi_c^T. \tag{A7}
$$

Finally, as $\Phi_i = \theta_i - \hat{\theta}_i$ and $\Phi_c = \theta_c - \hat{\theta}_c$, and the identification and control ideal parameters θ_i and θ_c are constant, we have that $\dot{\Phi}_i = -\dot{\hat{\theta}}_i$ and $\dot{\Phi}_c = -\dot{\hat{\theta}}_c$. Therefore, from (17) and (19), we have

$$
\dot{\phi}_c^T = -\left(S^T \nabla V_{e_c} \omega_c^T - S^T \varepsilon^T \Gamma_\varepsilon^{-1} + \sigma_c \hat{\theta}_c^T \right) \Gamma_c, \tag{A8}
$$

$$
\dot{\phi}_i^T = -\left(\omega_i^T \nabla V_{e_i} - \varepsilon^T \Gamma_\varepsilon^{-1} (P_1^T + \hat{\theta}_c P_2^T) + \sigma_i \hat{\theta}_i^T \right) \Gamma_i. \tag{A9}
$$

Stability Proof of the Error Dynamical Equations

The system composed by the errors dynamical Equations (A5), (A6), (A8) and (A9) has an associated Lyapunov function, which is positive and depends on the design energy function V_e.

$$
V(e_c, \Phi_c, e_i, \Phi_i) = V_{e_c} + \frac{1}{2} Trace(|B|\Phi_c^T \Gamma_c^{-1} \Phi_c) + V_{e_i} + \frac{1}{2} Trace(\Phi_i^T \Gamma_i^{-1} \Phi_i). \tag{A10}
$$

The first time derivative of (A10) gives

$$
\dot{V}(e_c, \Phi_c, e_i, \Phi_i) = \nabla V_{e_c}^T \dot{e}_c + Trace(|B|\dot{\Phi}_c^T \Gamma_c^{-1} \Phi_c) + \nabla V_{e_i}^T \dot{e}_i + Trace(\dot{\Phi}_i^T \Gamma_i^{-1} \Phi_i). \tag{A11}
$$

Substituting (A5) and (A6) into (A11), we obtain:

$$
\begin{aligned}
\dot{V}(e_c, \Phi_c, e_i, \Phi_i) = {} & \nabla V_{e_c}^T(-K_c e_c + B^T \phi_c^T \omega_c - \zeta) + Trace(|B|\dot{\Phi}_c^T \Gamma_c^{-1} \Phi_c) \\
& + \nabla V_{e_i}^T(-K_i e_i + \Phi_i^T \omega_i + \zeta) + Trace(\dot{\Phi}_i^T \Gamma_i^{-1} \Phi_i).
\end{aligned}
$$

Regrouping terms, it gives:

$$
\begin{aligned}
\dot{V}(e_c, \Phi_c, e_i, \Phi_i) = {} & -\nabla V_{e_c}^T K_c e_c + \nabla V_{e_c}^T B^T \phi_c^T \omega_c - \nabla V_{e_c}^T \zeta + Trace(|B|\dot{\Phi}_c^T \Gamma_c^{-1} \Phi_c) \\
& - \nabla V_{e_i}^T K_i e_i + \nabla V_{e_i}^T \Phi_i^T \omega_i + \nabla V_{e_i}^T \zeta + Trace(\dot{\Phi}_i^T \Gamma_i^{-1} \Phi_i).
\end{aligned}
$$

Substituting (A8) and (A9) into the last equation gives

$$
\begin{aligned}
\dot{V}(e_c, \Phi_c, e_i, \Phi_i) = {} & -\nabla V_{e_c}^T K_c e_c - \nabla V_{e_i}^T K_i e_i + \nabla V_{e_c}^T B^T \phi_c^T \omega_c + \nabla V_{e_i}^T \Phi_i^T \omega_i - \nabla V_{e_c}^T \zeta + \nabla V_{e_i}^T \zeta \\
& - Trace\left(\left(|B|S^T \nabla V_{e_c} \omega_c^T - |B|S^T \varepsilon^T \Gamma_\varepsilon + |B|\sigma_c \hat{\theta}_c^T \right) \Gamma_c \Gamma_c^{-1} \Phi_c \right) \\
& - Trace\left(\left(\omega_i^T \nabla V_{e_i} - \varepsilon^T \Gamma_\varepsilon^{-1}(P_1^T + \hat{\theta}_c P_2^T) + \sigma_i \hat{\theta}_i^T \right) \Gamma_i \Gamma_i^{-1} \Phi_i \right).
\end{aligned}
$$

Now, considering $|B|S^T = B$, $\Gamma_c \Gamma_c^{-1} = 1$ and $\Gamma_i \Gamma_i^{-1} = 1$, and regrouping terms, it follows that

$$
\begin{aligned}
\dot{V}(e_c, \Phi_c, e_i, \Phi_i) = {} & -\nabla V_{e_c}^T K_c e_c - \nabla V_{e_i}^T K_i e_i + \nabla V_{e_c}^T B^T \phi_c^T \omega_c + \nabla V_{e_i}^T \Phi_i^T \omega_i - \nabla V_{e_c}^T \zeta + \nabla V_{e_i}^T \zeta \\
& - Trace\left(B \nabla V_{e_c} \omega_c^T \Phi_c - B\varepsilon^T \Gamma_\varepsilon^{-1} \Phi_c + |B|\sigma_c \theta_c^T \Phi_c \right) \\
& - Trace\left(\omega_i^T \nabla V_{e_i} \Phi_i - \varepsilon^T \Gamma_\varepsilon^{-1}(P_1^T \Phi_i + \hat{\theta}_c P_2^T \Phi_i) + \sigma_i \hat{\theta}_i^T \Phi_i \right).
\end{aligned}
$$

Moreover, the authors consider the two vectors' properties, where $a^T b = Trace(ab^T)$, to write the terms $\nabla V_{e_c}^T B^T \phi_c^T \omega_c$ and $\nabla V_{e_i}^T \Phi_i^T \omega_i$ into the trace as follows:

$$\dot{V}(e_c, \Phi_c, e_i, \Phi_i) = - \nabla V_{e_c}^T K_c e_c - \nabla V_{e_i}^T K_i e_i$$
$$- \text{Trace}\left(-B\nabla V_{e_c}\omega_c^T \Phi_c + B\nabla V_{e_c}\omega_c^T \Phi_c - B\varepsilon^T \Gamma_\varepsilon^{-1}\Phi_c + |B|\sigma_c\theta_c^T\Phi_c + \zeta^T\nabla V_{e_c}\right)$$
$$- \text{Trace}\left(-\omega_i^T \nabla V_{e_i}\Phi_i + \omega_i^T \nabla V_{e_i}\Phi_i - \varepsilon^T \Gamma_\varepsilon^{-1}(P_1^T\Phi_i + \hat{\theta}_c P_2^T\Phi_i) + \sigma_i\hat{\theta}_i^T\Phi_i - \zeta^T\nabla V_{e_i}\right).$$

Simplifying the last equation, after canceling identical terms with opposite signs and regrouping the terms with $\varepsilon^T\Gamma_\varepsilon^{-1}$ conveniently to obtain Equation (A7), gives

$$\dot{V}(e_c, \Phi_c, e_i, \Phi_i) = - \nabla V_{e_c}^T K_c e_c - \nabla V_{e_i}^T K_i e_i - \text{Trace}\left(\varepsilon^T \Gamma_\varepsilon^{-1}\varepsilon\right)$$
$$- \text{Trace}\left(|B|\sigma_c\theta_c^T\Phi_c\right) - \text{Trace}\left(\zeta^T\nabla V_{e_c}\right) \quad \text{(A12)}$$
$$- \text{Trace}\left(\sigma_i\hat{\theta}_i^T\Phi_i\right) + \text{Trace}\left(\zeta^T\nabla V_{e_i}\right).$$

In this scenario, we assume that all parameters involved, K_c, K_i, $|B|$, σ_c, σ_i, and Γ_ε, are strictly positive. Additionally, we know that the parameters characterizing the plant, along with their first derivatives with respect to time, remain within certain bounds.

However, upon inspection of Equation (A12), it becomes evident that while the first terms indicate negativity, the signs of the subsequent four terms are not immediately discernible. To address this ambiguity, we aim to reformulate Equation (A12) using modulus and norm properties, as demonstrated in [38].

Using properties of the Frobenius norm and the Cauchy–Schwarz inequality where $Trace(ABC) \leq ||A||_F||B||_F||C||_F$, the terms become $-Trace(|B|\sigma_c\hat{\theta}_c^T\Phi_c) \leq |||B|\sigma_c||_F||\hat{\theta}_c^T||_F||\Phi_c||_F$, $-Trace(\sigma_i\hat{\theta}_i^T\Phi_i)) \leq ||\sigma_i||_F||\hat{\theta}_i^T||_F||\Phi_i||_F$, $Trace(\zeta^T\nabla V_{e_c}) \leq ||\zeta^T||_F||\nabla V_{e_c}||_F$ and $Trace(\zeta^T\nabla V_{e_i}) \leq ||\zeta^T||_F||\nabla V_{e_i}||_F$. Using the property $2ab \leq a^2 + b^2$, we have $-Trace(|B|\sigma_c\hat{\theta}_c^T\Phi_c) \leq \frac{1}{2}|||B|\sigma_c||_F(||\hat{\theta}_c^T||_F^2 + ||\Phi_c||_F^2)$, $-Trace(\sigma_i\hat{\theta}_i^T\Phi_i)) \leq \frac{1}{2}||\sigma_i||_F(||\hat{\theta}_i^T||_F^2 + ||\Phi_i||_F^2)$, $Trace(\zeta^T\nabla V_{e_c}) \leq \frac{1}{2}(||\zeta^T||_F^2 + ||\nabla V_{e_c}||_F^2)$ and $Trace(\zeta^T\nabla V_{e_i}) \leq \frac{1}{2}(||\zeta^T||_F^2||\nabla V_{e_i}||_F^2)$.

As a result, Equation (A12) becomes

$$\dot{V}(e_c, \Phi_c, e_i, \Phi_i) \leq -\nabla V_{e_c}^T K_c e_c - \nabla V_{e_i}^T K_i e_i - Trace(\varepsilon^T\Gamma_\varepsilon^{-1}\varepsilon)$$
$$- \frac{1}{2}|||B|\sigma_c||_F\left(||\hat{\theta}_c^T||_F^2 + ||\Phi_c||_F^2\right) - \frac{1}{2}\left(||\zeta^T||_F^2 + ||\nabla V_{e_c}||_F^2\right)$$
$$- \frac{1}{2}||\sigma_i||_F\left(||\hat{\theta}_i^T||_F^2 + ||\Phi_i||_F^2\right) + \frac{1}{2}\left(||\zeta^T||_F^2 + ||\nabla V_{e_i}||_F^2\right).$$

which equals a hyperelliptic paraboloid of parameter r:

$$\dot{V}(e_c, \Phi_c, e_i, \Phi_i) = -\nabla V_{e_c}^T K_c e_c - \nabla V_{e_i}^T K_i e_i - Trace(\varepsilon^T\Gamma_\varepsilon^{-1}\varepsilon) + r^2$$
$$- \frac{1}{2}|||B|\sigma_c||_F\left(||\hat{\theta}_c^T||_F^2 + ||\Phi_c||_F^2\right) - \frac{1}{2}\left(||\zeta^T||_F^2 + ||\nabla V_{e_c}||_F^2\right)$$
$$- \frac{1}{2}||\sigma_i||_F\left(||\hat{\theta}_i^T||_F^2 + ||\Phi_i||_F^2\right) + \frac{1}{2}\left(||\zeta^T||_F^2 + ||\nabla V_{e_i}||_F^2\right).$$

Therefore, $\dot{V} \leq 0$ only outside the region Ω, which is the following instability hyperelliptic paraboloid that is compact, closed, and includes the following origin:

$$\Omega = \frac{1}{2}|||B|\sigma_c||_F\left(||\hat{\theta}_c^T||_F^2 + ||\Phi_c||_F^2\right) + \frac{1}{2}\left(||\zeta^T||_F^2 + ||\nabla V_{e_c}||_F^2\right)$$
$$\frac{1}{2}||\sigma_i||_F\left(||\hat{\theta}_i^T||_F^2 + ||\Phi_i||_F^2\right) - \frac{1}{2}\left(||\zeta^T||_F^2 + ||\nabla V_{e_i}||_F^2\right) \leq r^2.$$

Hence, using Lyapunov's second method, it can be concluded that the variables of the closed-loop dynamical Equations (A5), (A6), (A8) and (A9) are bounded outside Ω. In case

the errors take small enough values that result in $\dot{V} \leq 0$ (inside the instability compact and closed region Ω, including the origin); these will be pushed back to a stable boundary. In practice, the values of σ_c, σ_i, Γ_c, Γ_i, and Γ_ε are chosen so that the permanent errors are as a small as possible, as can be seen in the following section.

Thus, $e_c(t)$, $e_i(t)$, $\Phi_c(t)$, and $\Phi_i(t)$ are bounded outside Ω, i.e., $e_c(t)$, $e_i(t)$, $\Phi_c(t)$, and $\Phi_i(t) \in L^\infty$ outside Ω. Since $e_c = y^* - y$ and $e_i = y - \hat{y}$ are bounded, it implies that y, $\hat{y}$ and are bounded as y^* is a bounded reference. As $\Phi_c(t)$ and $\Phi_i(t)$ are bounded, and we have bounded plant parameters, then the adaptive parameters θ_c and θ_i are bounded, since $\hat{\theta}_i = \theta_i - \Phi_i$ and $\hat{\theta}_c = \theta_c - \Phi_c$. Having all these bounded signals outside Ω, and that V, $e_c(t)$, $e_i(t)$, $\Phi_c(t)$ and $\Phi_i(t) \in L^\infty$, from (A5), (A6), (A8) and (A9), we have that $\dot{e}_c(t)$, $\dot{e}_i(t)$, $\dot{\Phi}_c(t)$ and $\dot{\Phi}_i(t) \in L^\infty$.

Integrating both sides of $\dot{V}(e_c, \Phi_c, e_i, \Phi_i)$ in the interval $(0, \infty)$ gives

$$
\begin{aligned}
V(\infty) - V(0) = \int_0^\infty \Big(&-\nabla V_{e_c}^T K_c e_c - \nabla V_{e_i}^T K_i e_i - Trace(\varepsilon^T \Gamma_\varepsilon^{-1} \varepsilon) + r^2 \\
&- \frac{1}{2} |||B|\sigma_c||_F \Big(||\hat{\theta}_c^T||_F^2 + ||\Phi_c||_F^2 \Big) - \frac{1}{2} \Big(||\zeta^T||_F^2 + ||\nabla V_{e_c}||_F^2 \Big) \\
&- \frac{1}{2} ||\sigma_i||_F \Big(||\hat{\theta}_i^T||_F^2 + ||\Phi_i||_F^2 \Big) + \frac{1}{2} \Big(||\zeta^T||_F^2 + ||\nabla V_{e_i}||_F^2 \Big) \Big) d\tau
\end{aligned}
$$

as V is bounded outside Ω, from the right-hand side of this last equation, we have $e_c(t)$ and $e_i(t) \in L^2$ outside Ω.

Furthermore, as $e_c(t)$, $\dot{e}_c(t) \in L^\infty$ and $e_c(t) \in L^2$, and $e_i(t)$, $\dot{e}_i(t) \in L^\infty$ and $e_i(t) \in L^2$, all outside Ω, using Barbalat´s Lemma [30] (Section 4.5.2) we have that $e_c(t)$ and $e_i(t)$, both tend asymptotically to zero outside Ω. Hence, $y(t) \to y^*$ and $\hat{y}(t) \to y(t)$ outside Ω^C. We do not ensure parameter convergence. This concludes the proof. $\lozenge$

References

1. Ivanov-Smolenskij, A.; Kuznecov, B. *Electrical Machines: Vol. 1*; Mir: Moscow, Russia, 1983.
2. Hannan, M.; Ali, J.A.; Mohamed, A.; Hussain, A. Optimization techniques to enhance the performance of induction motor drives: A review. *Renew. Sustain. Energy Rev.* **2018**, *81*, 1611–1626. [CrossRef]
3. Travieso-Torres, J.C.; Contreras-Jara, C.; Diaz, M.; Aguila-Camacho, N.; Duarte-Mermoud, M.A. New Adaptive Starting Scalar Control Scheme for Induction Motor Variable Speed Drives. *IEEE Trans. Energy Convers.* **2021**, *37*, 729–736. [CrossRef]
4. Depenbrock, M. Direkte selbstregelung (DSR) für hochdynamische drehfeldantriebe mit stromrichterspeisung. *etz-Archiv* **1985**, *7*, 211–218.
5. Vas, P. Sensorless Vector and Direct Torque Control. *Oxf. Univ. Press Google Sch.* **1998**, *2*, 265–273.
6. Hasse, K. Zur Dynamic Drehzahlgeregelter Antriebe mit Stromaschinen. Ph.D. Thesis, Technische Hochschule Darmstadt, Darmstadt, Germany, 1969.
7. Blaschke, F. The principle of field orientation as applied to the new transvector closed-loop control system for rotating-field machine. *Siemens Rev.* **1772**, *34*, 217–220.
8. Desoer, C.; Lin, C.A. Tracking and disturbance rejection of MIMO nonlinear systems with PI controller. *IEEE Trans. Autom. Control* **1985**, *30*, 861–867. [CrossRef]
9. Ogata, K. *Ingeniería de Control Moderna*; Pearson Educación: London, UK, 2003.
10. Sengamalai, U.; Anbazhagan, G.; Thamizh Thentral, T.; Vishnuram, P.; Khurshaid, T.; Kamel, S. Three phase induction motor drive: A systematic review on dynamic modeling, parameter estimation, and control schemes. *Energies* **2022**, *15*, 8260. [CrossRef]
11. Amaral, G.F.V.; Baccarini, J.M.R.; Coelho, F.C.R.; Rabelo, L.M. A high precision method for induction machine parameters estimation from manufacturer data. *IEEE Trans. Energy Convers.* **2020**, *36*, 1226–1233. [CrossRef]
12. Perin, M.; Pereira, L.A.; Silveira, G.B.; Haffner, S. Estimation of the parameters for multi-cage models of induction motors using manufacturer data and PSO. In *Electrical Engineering*; Springer: Berlin/Heidelberg, Germany, 2023; pp. 1–19.
13. Engineers, E.; Board, I. *112-2017—IEEE Standard Test Procedure for Polyphase Induction Motors and Generators*; IEEE: Piscataway, NJ, USA, 2018; pp. 1–115. [CrossRef]
14. Yoo, J.; Lee, J.H.; Sul, S.K. FEA-Assisted Experimental Parameter Map Identification of Induction Motor for Wide-Range Field-Oriented Control. *IEEE Trans. Power Electron.* **2023**, *39*, 1353–1363. [CrossRef]
15. Véliz-Tejo, A.; Travieso-Torres, J.C.; Peters, A.A.; Mora, A.; Leiva-Silva, F. Normalized-Model Reference System for Parameter Estimation of Induction Motors. *Energies* **2022**, *15*, 4542. [CrossRef]
16. Travieso-Torres, J.C.; Lee, S.S.; Veliz-Tejo, A.; Leiva-Silva, F.; Ricaldi-Morales, A. Self-Commissioning Parameter Estimation Algorithm for Loaded Induction Motors. *IEEE Trans. Ind. Electron.* **2024**, 1–11. [CrossRef]

17. Travieso-Torres, J.C.; Duarte-Mermoud, M.A. Two simple and novel SISO controllers for induction motors based on adaptive passivity. *ISA Trans.* **2008**, *47*, 60–79. [CrossRef] [PubMed]
18. Talla, J.; Leu, V.Q.; Šmídl, V.; Peroutka, Z. Adaptive speed control of induction motor drive with inaccurate model. *IEEE Trans. Ind. Electron.* **2018**, *65*, 8532–8542. [CrossRef]
19. Kilic, E.; Ozcalik, H.R.; Yilmaz, S. Efficient speed control of induction motor using RBF based model reference adaptive control method. *Autom. Časopis Za Autom. Mjer. Elektron. Računarstvo I Komun.* **2016**, *57*, 714–723. [CrossRef]
20. Zellouma, D.; Bekakra, Y.; Benbouhenni, H. Field-oriented control based on parallel proportional–integral controllers of induction motor drive. *Energy Rep.* **2023**, *9*, 4846–4860. [CrossRef]
21. Sudheer, A.; Aware, M.V. Improved fractional order speed controller with non-linear vsi-im model to enhance the load disturbance capability. *ISA Trans.* **2023**, *142*, 538–549. [CrossRef] [PubMed]
22. Aziz, A.G.M.A.; Abdelaziz, A.Y.; Ali, Z.M.; Diab, A.A.Z. A comprehensive examination of vector-controlled induction motor drive techniques. *Energies* **2023**, *16*, 2854. [CrossRef]
23. Adigintla, S.; Aware, M.V. Robust fractional order speed controllers for induction motor under parameter variations and low speed operating regions. *IEEE Trans. Circuits Syst. II Express Briefs* **2022**, *70*, 1119–1123. [CrossRef]
24. Zellouma, D.; Bekakra, Y.; Benbouhenni, H. Robust synergetic-sliding mode-based-backstepping control of induction motor with MRAS technique. *Energy Rep.* **2023**, *10*, 3665–3680. [CrossRef]
25. Ali, S.; Prado, A.; Pervaiz, M. Hybrid backstepping-super twisting algorithm for robust speed control of a three-phase induction motor. *Electronics* **2023**, *12*, 681. [CrossRef]
26. Yang, G.; Yao, J. Multilayer neurocontrol of high-order uncertain nonlinear systems with active disturbance rejection. *Int. J. Robust Nonlinear Control* **2024**, *34*, 2972–2987. [CrossRef]
27. Travieso-Torres, J.C.; Duarte-Mermoud, M.A.; Díaz, M.; Contreras-Jara, C.; Hernández, F. Closed-Loop Adaptive High-Starting Torque Scalar Control Scheme for induction Motor Variable Speed Drives. *Energies* **2022**, *15*, 3489. [CrossRef]
28. Ioannou, P.A.; Sun, J. *Robust Adaptive Control*; PTR Prentice-Hall: Upper Saddle River, NJ, USA, 1996; Volume 1.
29. Åström, K.J.; Wittenmark, B. *Adaptive Control*; Courier Corporation: North Chelmsford, MA, USA, 2008.
30. Narendra, K.; Annaswamy, A. *Stable Adaptive Systems*; Dover Books on Electrical Engineering; Dover Publications: Mineola, NY, USA, 2012.
31. Tiwari, M.; Prazenica, R.; Henderson, T. Direct adaptive control of spacecraft near asteroids. *Acta Astronaut.* **2023**, *202*, 197–213. [CrossRef]
32. Artuc, M.B.; Bayezit, I. Robust adaptive quadrotor position tracking control for uncertain and fault conditions. *Proc. Inst. Mech. Eng. Part G J. Aerosp. Eng.* **2023**, *237*, 3172–3184. [CrossRef]
33. Wang, Y.; Shen, C.; Huang, J.; Chen, H. Model-free adaptive control for unmanned surface vessels: A literature review. *Syst. Sci. Control Eng.* **2024**, *12*, 2316170. [CrossRef]
34. Liu, Z.; Zhao, Y.; Zhang, O.; Chen, W.; Wang, J.; Gao, Y.; Liu, J. A Novel Faster Fixed-Time Adaptive Control for Robotic Systems With Input Saturation. *IEEE Trans. Ind. Electron.* **2023**, *71*, 5215–5223. [CrossRef]
35. Burghi, T.; Iossaqui, J.; Camino, J. A general update rule for Lyapunov-based adaptive control of mobile robots with wheel slip. *Int. J. Adapt. Control Signal Process.* **2024**, *38*, 1172–1198. [CrossRef]
36. Mirzaee, M.; Kazemi, R. Direct adaptive fractional-order non-singular terminal sliding mode control strategy using extreme learning machine for position control of 5-DOF upper-limb exoskeleton robot systems. *Trans. Inst. Meas. Control* **2024**, 01423312231225605. [CrossRef]
37. Abubakr, H.; Vasquez, J.C.; Mohamed, T.H.; Guerrero, J.M. The concept of direct adaptive control for improving voltage and frequency regulation loops in several power system applications. *Int. J. Electr. Power Energy Syst.* **2022**, *140*, 108068. [CrossRef]
38. Travieso-Torres, J.C.; Ricaldi-Morales, A.; Véliz-Tejo, A.; Leiva-Silva, F. Robust Cascade MRAC for a Hybrid Grid-Connected Renewable Energy System. *Processes* **2023**, *11*, 1774. [CrossRef]
39. Karami-Mollaee, A.; Barambones, O. Higher Order Sliding Mode Control of MIMO Induction Motors: A New Adaptive Approach. *Mathematics* **2023**, *11*, 4558. [CrossRef]
40. Çavuş, B.; Aktaş, M. A New Adaptive Terminal Sliding Mode Speed Control in Flux Weakening Region for DTC Controlled Induction Motor Drive. *IEEE Trans. Power Electron.* **2023**, *39*, 449–458. [CrossRef]
41. Duarte, M.A.; Narendra, K.S. Combined direct and indirect approach to adaptive control. *IEEE Trans. Autom. Control* **1989**, *34*, 1071–1075. [CrossRef]
42. Duarte-Mermoud, M.A.; Rojo, F.A.; Pérez, R. Experimental evaluation of combined model reference adaptive controller in a pH regulation process. *Int. J. Adapt. Control Signal Process.* **2002**, *16*, 85–106. [CrossRef]
43. Duarte-Mermoud, M.A.; Rioseco, J.S.; González, R.I. Control of longitudinal movement of a plane using combined model reference adaptive control. *Aircr. Eng. Aerosp. Technol.* **2005**, *77*, 199–213. [CrossRef]
44. Lavretsky, E. Combined/composite model reference adaptive control. *IEEE Trans. Autom. Control* **2009**, *54*, 2692–2697. [CrossRef]
45. Xie, J.; Yan, H.; Li, S.; Yang, D. Almost output regulation model reference adaptive control for switched systems: Combined adaptive strategy. *Int. J. Syst. Sci.* **2020**, *51*, 556–569. [CrossRef]
46. Roy, S.B.; Bhasin, S.; Kar, I.N. Combined MRAC for unknown MIMO LTI systems with parameter convergence. *IEEE Trans. Autom. Control* **2017**, *63*, 283–290. [CrossRef]

47. Makavita, C.D.; Nguyen, H.D.; Ranmuthugala, D.; Jayasinghe, S.G. Composite model reference adaptive control for an unmanned underwater vehicle. *Underw. Technol.* **2015**, *33*, 81–93. [CrossRef]

48. Abdul Ghaffar, A.F.; Richardson, T.; Greatwood, C. A combined model reference adaptive control law for multirotor UAVs. *IET Control Theory Appl.* **2021**, *15*, 1474–1487. [CrossRef]

49. Vas, P. *Electrical Machines and Drives: A Space-Vector Theory Approach*; Clarendon Press Oxford: Oxford, UK, 1992; Volume 1.

50. Park, R.H. Two-reaction theory of synchronous machines generalized method of analysis-part I. *Trans. Am. Inst. Electr. Eng.* **1929**, *48*, 716–727. [CrossRef]

51. Dorf, R.C.; Bishop, R.H. *Modern Control Systems*; Pearson Education, Inc.: Upper Saddle River, NJ, USA, 2011.

52. Siemens. *Vector Control Simovert Masterdrives VC, Single-Motor and Multi-Motor Drives 0.55 kW to 2300 kW, Catalog DA 65.10 • 2003/2004*; Siemens AG: Berlin/Heidelberg, Germany, 2003.

53. Schiff, J.L. *The Laplace Transform: Theory and Applications*; Springer Science & Business Media: Berlin/Heidelberg, Germany, 1999.

54. Travieso-Torres, J.C.; Contreras, C.; Hernández, F.; Duarte-Mermoud, M.A.; Aguila-Camacho, N.; Orchard, M.E. Adaptive passivity-based control extended for unknown control direction. *ISA Trans.* **2022**, *122*, 398–408. [CrossRef] [PubMed]

55. Feraga, C.E.; Sedraoui, M.; Bachir Bouiadjra, R. Enhanced Indirect Field-Oriented Control of Single-Phase Induction Motor Drive Using H∞ Current Controller. *Arab. J. Sci. Eng.* **2019**, *44*, 7187–7202. [CrossRef]

56. Cao, P.; Zhang, X.; Yang, S. A unified-model-based analysis of MRAS for online rotor time constant estimation in an induction motor drive. *IEEE Trans. Ind. Electron.* **2017**, *64*, 4361–4371. [CrossRef]